Phase transformations and phase equilibria in the La−Ni and La−Ni−Fe systems. Part 1: Liquidus & solidus projections

I. Fartushna [a, *], M. Mardani [a], I. Bajenova [a], A. Khvan [a], V. Cheverikin [a], K.W. Richter [b], A. Kondratiev [a]

[a] *Thermochemistry of Materials Scientific Research Centre, NUST MISIS, Moscow, Russia*
[b] *University of Vienna, Faculty of Chemistry, Vienna, Austria*

ARTICLE INFO

ABSTRACT

Phase equilibria in the La−Ni and La−Ni−Fe systems were studied using DTA, X-ray diffraction, SEM and EPMA. La−Ni phase diagram, liquidus and solidus projections, melting diagram and a Scheil reaction scheme for the La−Ni−Fe system over the whole concentration range were constructed. Among binary compounds $LaNi_5$, La_5Ni_{19} and La_2Ni_7 have large homogeneity ranges and dissolve at the solidus temperature up to 21.9, 16.1 and 14.0 at.% Fe, respectively. The homogeneity ranges of the remaining phases are smaller. No ternary compounds have been identified in the La−Ni−Fe system. Liquidus projection is characterized by 13 fields of primary solidification of the component-based solid solutions (γFe,Ni), (δFe), (αFe), (βLa), (γLa) and solid solutions based on binary phases $LaNi_5$, La_5Ni_{19}, La_2Ni_7, $LaNi_3$, La_7Ni_{16}, La_2Ni_3, $LaNi$, La_7Ni_3 and La_3Ni. The solidus projection is characterized by ten three-phase fields, which result from invariant four-phase equilibria, three are of eutectic type and seven of transition type.

© 2020 Elsevier B.V. All rights reserved.

1. Introduction

The intermetallic compounds composed from rare earth elements (R) and transition metals (TM) are of particular interest due to their potential application as highly demanded functional materials, such as permanent magnets and hydrogen-storage materials [1]. The RNi_5 (R = light rare earth) compounds are exchange enhanced Pauli paramagnets at all temperatures. Replacement of Ni by Fe in RNi_5 phases expands the lattice and produces a significant alteration in magnetic behavior [2]. Using solid solutions based on binary R-TM compounds, it is possible to vary the materials properties in the desired way. However, to understand the reactions during production of these magnets, the detailed knowledge of the third element influence on the phase equilibria and the homogeneity ranges of the intermetallic phases are needed. Therefore, the phase diagram of La−Ni−Fe system is an important theoretical basis for new materials design and processing. However, data on phase equilibria and types of transformations in this system are very limited. At the same time, information on the phase equilibria during crystallization is absent. In order to continue our

experimental studies on the R-Fe-TM and R-Fe-C ternary systems (TM = Mn, Co, Ni; R = La, Ce) [3−14] we have carried out an investigation of phase equilibria in the La−Fe−Ni system during solidification over the whole range of compositions. The results of the study allow us to evaluate the prospects of their further, deeper study, with a view to suggest practical applications in the modern industry.

2. Literature review

A brief summary of the literature data concerning phase equilibria of the ternary La−Ni−Fe system and its binary subsystems is presented below.

2.1. Binary La−Fe system

The La−Fe phase diagram reported by Mardani et al. [3] was adopted in the current work. This system is of a simple eutectic type with the eutectic reaction $L \rightleftarrows (\alpha Fe) + (\beta La)$ at 788 °C and 88 at.% La and there is no stable miscibility gap forming in the liquid phase of the La−Fe system. The allotropic transformation $(\delta Fe) \rightleftarrows (\gamma Fe)$ proceeds by the metatectic reaction $(\delta Fe) \rightleftarrows L + (\gamma Fe)$ at 1383 °C and ~50 at.% La [3]. The $(\gamma Fe) \rightleftarrows (\alpha Fe)$ transformation occurs by a peritectic reaction $L + (\gamma Fe) \rightleftarrows (\alpha Fe)$ at 918 °C and ~80 at.% La [3].

* Corresponding author.
E-mail address: juliefart@mail.ru (I. Fartushna).

2.2. Binary Fe−Ni system

The phase diagram of the Fe−Ni system was adopted in this work according to a thermodynamic assessment [15]. The following phases form in this system: (δFe)-phase (a high-temperature iron-based solid solution); (γFe,Ni)-phase (a continuous solid solution between Ni and Fe); (αFe)-phase (a low-temperature iron-based solid solution); FeNi₃ (an ordered cubic phase with Cu₃Au-type structure). The (γFe,Ni)-phase occupies wide temperature-composition region. There is a minimum on the liquidus and solidus curves of the (γFe,Ni) phase. The maximum solubility of Ni in (δFe) and (αFe) is 3.5 and 6.4 at.%, respectively.

The low-temperature part of the system was discussed in detail in Ref. [16,17]. FeNi₃ forms congruently from the (γFe,Ni) phase at 514 °C and demonstrates a considerable solubility range. The monotectoid equilibrium $(\gamma Fe,Ni)_{PM} = (\gamma Fe,Ni)_{FM} + (\alpha Fe)$ occurs at 428 °C. The $(\gamma Fe,Ni)_{FM}$ phase decomposes into (αFe) and FeNi₃ at 353 °C by the eutectoid reaction.

2.3. Binary La−Ni system

The binary La−Ni system was experimentally investigated by several authors [18−22] and a number of assessments of this system are available in the literature [23−25]. The recent version of the diagram [25] indicates that nine intermetallic phases, La₃Ni, La₇Ni₃, LaNi, La₂Ni₃, La₇Ni₁₆, LaNi₃, La₂Ni₇, La₅Ni₁₉ and LaNi₅, exist in the equilibrium state. The LaNi₅, LaNi, La₇Ni₃ and La₃Ni phases melt congruently at temperatures of 1357, 702, 537, and 542 °C, respectively, while the remaining compounds are formed by the peritectic reactions at 1003, 974, 811, 714 and 688 °C, respectively [25].

The first systematic study of the La−Ni phase diagram was carried out by Vogel and Fülling [18], who found six intermetallic compounds: La₃Ni, LaNi, LaNi₂, LaNi₃, LaNi₄ and LaNi₅. Later in Ref. [26,27] the composition LaNi₄ was corrected to La₂Ni₇. Buschow and Mal [19] reinvestigated the La−Ni system in the range 50−100 at.% Ni and observed a new phase with an approximate composition of LaNi₁.₄, which was later found to be La₂Ni₃ [28]. The phase diagram of La−Ni system was later studied by Ivanchenko et al. [20] in the whole concentration region. Zhang et al. [21] investigated this system over the composition range 50−83.3 at.% Ni and confirmed that the LaNi₂ phase cannot exist as a stable equilibrium phase. The LaNi₂.₂₈₆ phase [21,29] exists instead of LaNi₂, which was identified as La₇Ni₁₆. Later Yamamoto et al. [30] found a new La₅Ni₁₉ phase. The existence of this phase at high temperatures was also reported later in work [31]. Dischinger and Schaller [22] reported a new binary compound La₄Ni₁₇, which, however, has not been confirmed by other researchers [18−22].

The La₂Ni₇ compound exists in two polymorphic modifications: with the rhombohedral structure of the Gd₂Co₇ type (high temperature modification) and with the hexagonal structure of the Ce₂Ni₇ type (low temperature modification) [27] however, the transformation temperature is unknown.

Five eutectics are also present in the La−Ni system: L ⇌ LaNi₅ + (Ni) at 1541 K and 91.6 at.% Ni, L ⇌ La₂Ni₃ + LaNi at 948 K and 54.8 at.% Ni, L ⇌ La₇Ni₃ + LaNi at 790 K and 34.9 at.% Ni, L ⇌ La₇Ni₃ + La₃Ni at 803 K and 25.2 at.% Ni and L ⇌ (βLa) + La₃Ni at 798 K and 20.1 at.% Ni [25]. However, the temperatures of most eutectics according to various authors differ significantly.

It should be noted that there are several versions of the La−Ni binary phase diagram. For example, the peritectic reactions' temperatures for the formation of LaNi₃ and La₂Ni₇ phases were reported to be 967 and 1007 °C, respectively, in the work [20], while they were measured as 955 and 995 °C in the work [19]. At the same time Zhang et al. [21] suggests 811 °C as peritectic reaction

temperature for the formation of LaNi₃ phase, and 1014 and 976 °C as the temperatures for the formation of La₂Ni₇ phase and its polymorphic transformation, respectively.

Another La−Ni phase diagram was proposed in Ref. [25,30,31]. The main difference in comparison with other works is the presence of the La₅Ni₁₉ phase [30] in the system. According to Ref. [31] the peritectic reaction temperature for the formation of this phase was 1014 °C, while according to Zhang et al. [21], the temperature 1014 °C correspond to the temperature for the formation of La₂Ni₇ phase. Moreover, according to Refs. [30,31] the La₅Ni₁₉ phase is not stable at low temperatures and decomposes into La₂Ni₇ and LaNi₅ phases at temperature between 900 and 1000 °C, while according to An et al. [25] this phase is stable at low temperatures. It was reported in Ref. [32] that La₅Ni₁₉ has a hexagonal structure of the Pr₅Co₁₉ type. However, in Ref. [31,33] was reported that this phase has a rhombohedral structure of the Ce₅Co₁₉ type and that the hexagonal structure is metastable.

Another La−Ni phase diagram was reported by Dischinger and Schaller [22]. An essential difference from all the other works is the existence of La₄Ni₁₇. Moreover, some invariant reaction temperatures differ by more than 40 °C. It should be noted also that in Ref. [19−21,31], the homogeneity range of LaNi₅ was taken into account, while in Refs. [22,24,25,34] it was assumed that LaNi₅ is a stoichiometric compound. All these disagreements indicate that the additional experimental study on the determination of the phase equilibria in the La−Ni system needs to be carried out.

2.4. Ternary La−Ni−Fe system

The first experimental study of the La−Ni−Fe system was carried out in Ref. [35], in which the phase equilibria in the system at 400 °C were studied by XRD and SEM and an isothermal cross section was constructed at this temperature in the entire concentration range. It should be noted that the La₅Ni₁₉ compound was not found in Ref. [35]. This phase was found later in Ref. [30]. In addition, the LaNi₂ compound was later identified as La₇Ni₁₆.

In [36], phase equilibria in the Fe−Ni-16.7 at.% La system were studied using powder X-ray diffraction and differential thermal analysis, and isopleths at 16.7 at.% La was constructed. A new ternary compound Fe₂Ni₃La with a hexagonal structure and lattice parameters $a = 5.097(5)$, $c = 8.255(6)$ Å was found, which, however, was not observed in Ref. [35] and which was not confirmed later in Refs. [37].

Phase equilibria in La−Ni−Fe system were also studied in Ref. [37] using the methods of powder X-ray diffraction, differential thermal analysis, optical microscopy, and scanning electron microscopy. Partial isothermal sections of the system are proposed at 400 °C (in La-rich La region) and at 550 °C (in Ni-rich region). However, it should be noted that the compounds La₃Ni and La₅Ni₁₉ were not found in this work.

3. Experimental methods

3.1. Sample preparation

The samples were melted from starting materials with the purity of La−99.9%, Ni−99.9%, Fe−99.99% in an arc-furnace with an inconsumable tungsten electrode on a water-cooled copper hearth in an Ar atmosphere which was purified additionally by a Ti-melt. The samples were remelted 4−5 times to ensure their chemical homogeneity. The weight loss was less than 0.2%. The ingot weight was 3 g. The composition of each sample was analyzed by microprobe analysis and resulted in good conformity with the composition of the initial alloy mixture.

Samples were annealed in a tube furnace (Nabertherm RHTV
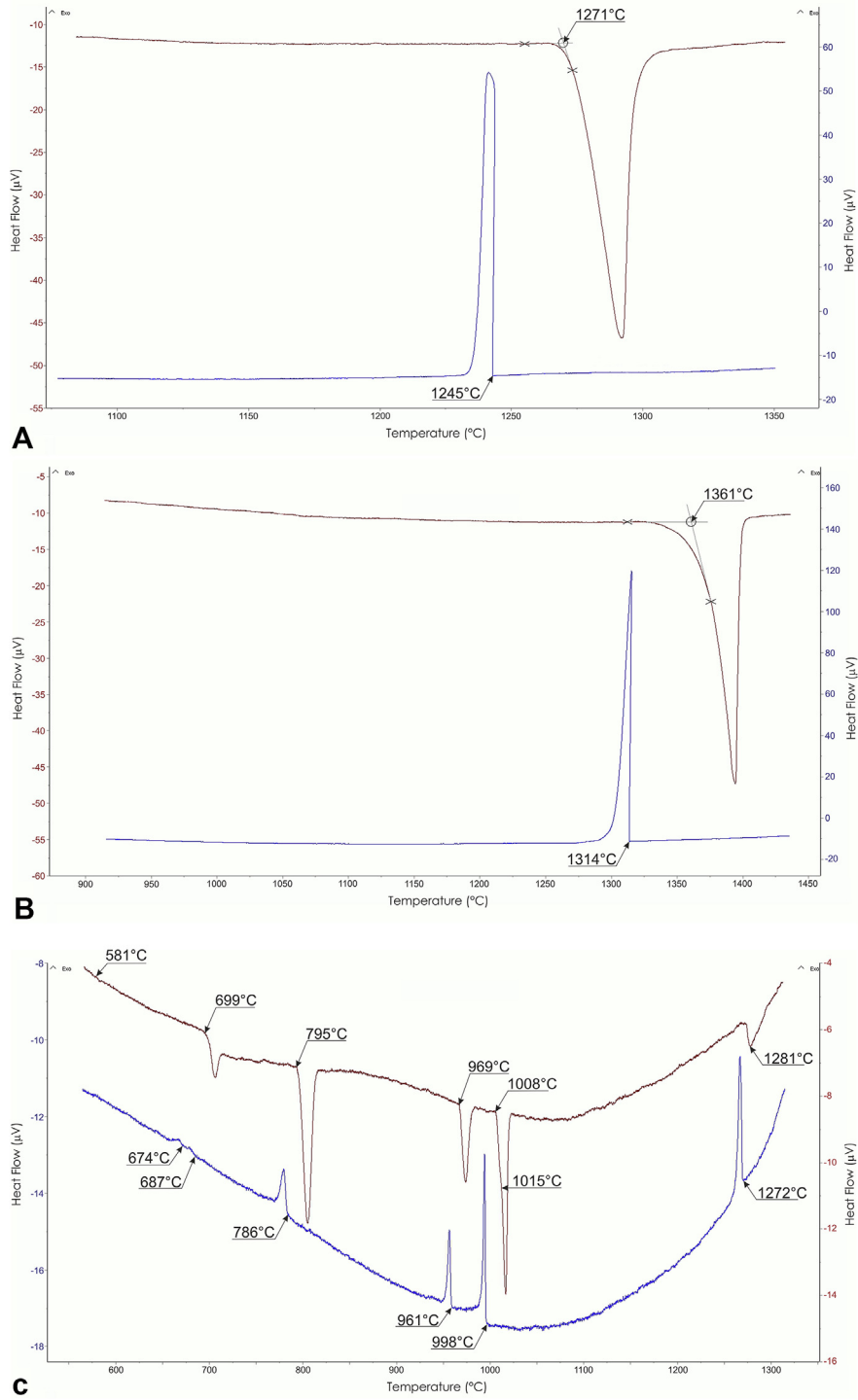
Fig. 1. DTA curve for La−Ni alloys:
a − 8.5La-91.5Ni, as-cast;
b − 16La−84Ni, annealed at 1250 °C/2 h;
c − 26.5La-73.5Ni, as-cast;
d − 32La−68Ni, as-cast;
e − 45La−55Ni, as-cast;
f − 65La−35Ni, as-cast;
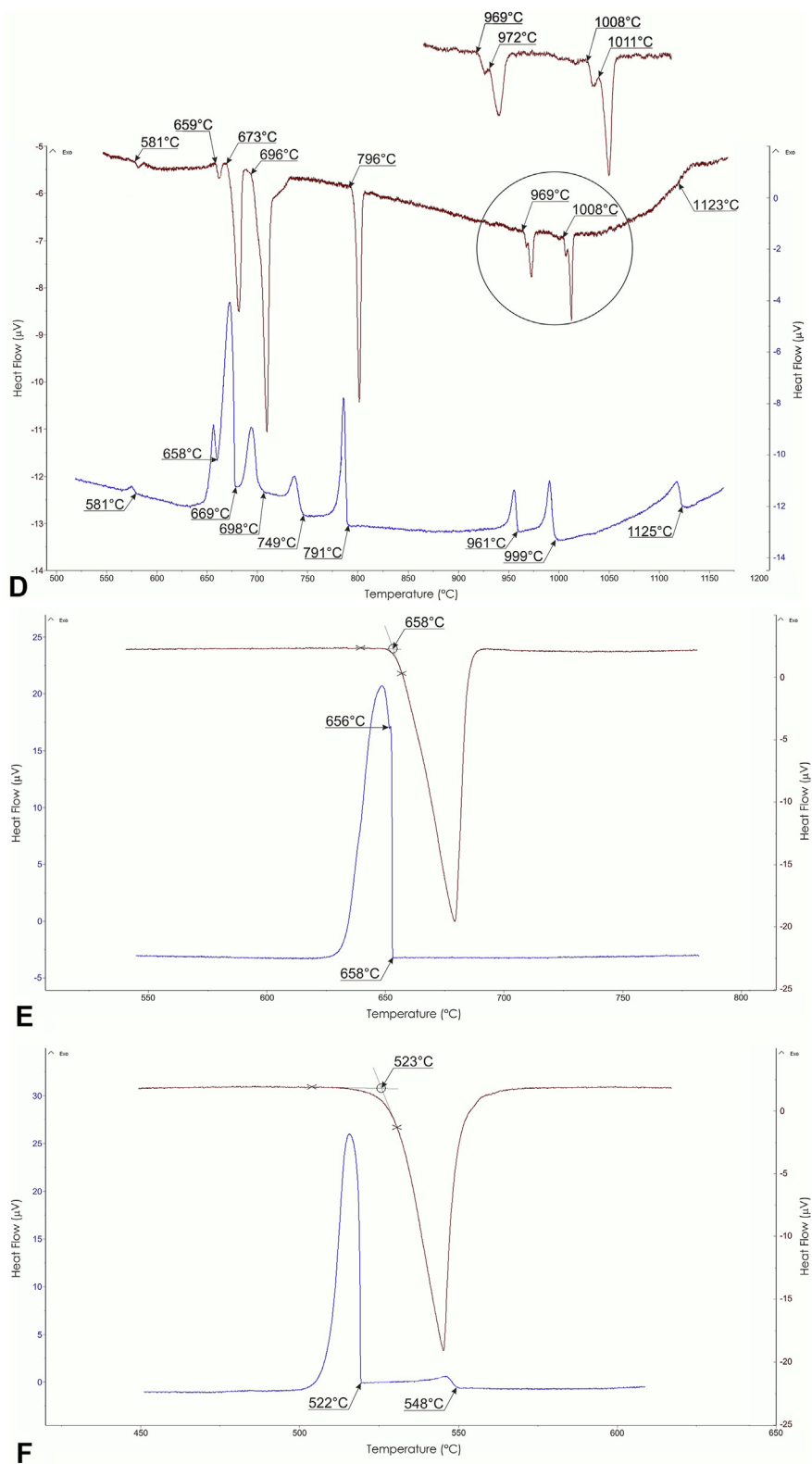g − 74.5La-25.5Ni, as-cast;
h − 77La−23Ni, as-cast.
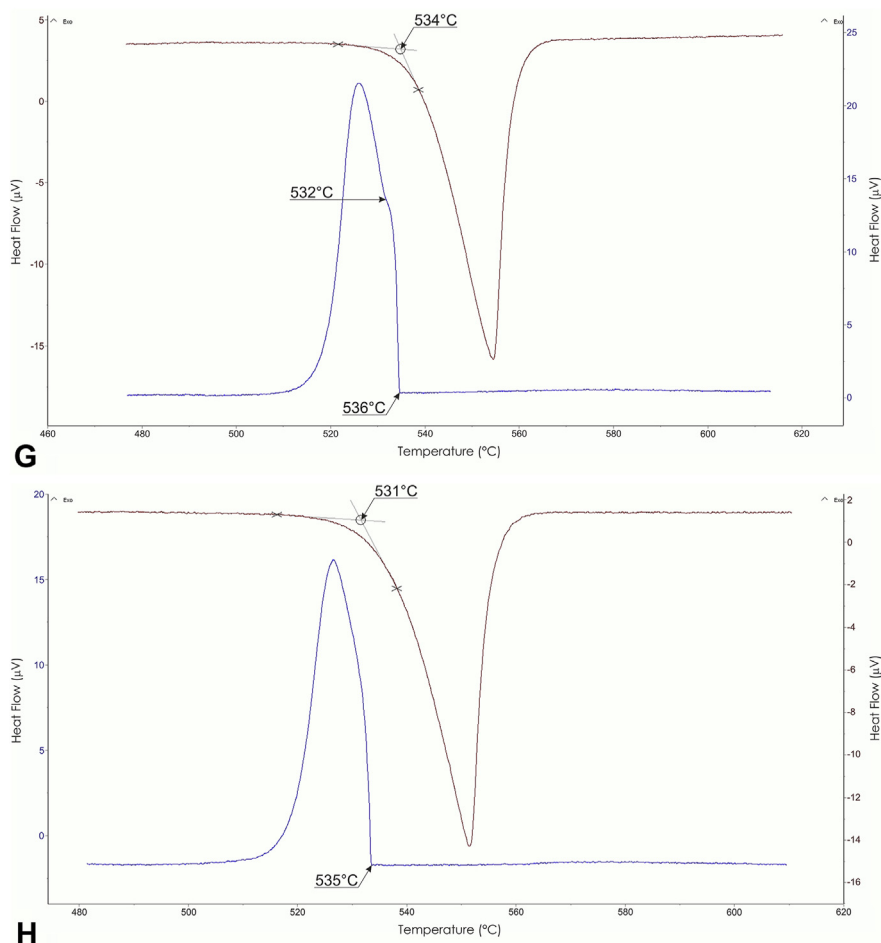
Fig. 1. (*continued*).

Fig. 1. (*continued*).

3.2. Microstructure analysis

Samples for microstructure analysis were prepared with a grinding and polishing machine (Struers Labopol-5, Denmark). The grinding was carried out with SiC-paper, and it was followed by polishing with diamond discs with grain sizes of 9, 3 and 1 μm respectively. Diamond suspension was applied at regular intervals during the preparation.

Prepared samples were examined with optical microscopy (OM) (Olympus-GX71F-5, UK) and scanning electron microscopy (SEM) using a TESCAN VEGA LMH, Czech Republic microscope with a LaB_6 cathode and an energy dispersive X-ray microanalysis system — Oxford Instruments Advanced AZtecEnergy, UK. For analysis, both backscattered electron and secondary electron imaging were used. A four-crystal wave spectrometer was used during the electron probe microanalysis (EPMA) of all the phases (the analyzed particle size was larger than 2 μm). 20 kV was set for the EPMA acceleration voltage. The measurement error in determining the concentration of elements using the X-ray analysis was 0.1 wt%. SEM analysis of the samples with high La content was carried out directly after polishing, to ensure that the samples did not have enough time to react with oxygen.

120/300/1700, Germany) with temperature accuracy of $\pm 3°C$, in Ar atmosphere. The samples were placed in an Al_2O_3 crucible and additionally covered by titanium chips to avoid oxidation. After the annealing some samples were quenched in oil to retain the equilibrium microstructures.

3.3. Differential thermal analysis

DSC LABSYS evo Setaram, France was used to measure the phase transition temperatures of the alloys. For calibration, pure metal standards: Sn (99.9995%), Pb (99.9995%), Al (99.995%), Ag (99.99%), Cu (99.999%) and Ni (99.99%) were used. DTA samples were placed in an Al_2O_3 crucible and the experiments were carried out under a flow of argon with 99.998% purity on the as-cast samples. The heating and cooling rates were 5 and 10 °C/min. For some alloys, the heating and cooling rate was 2 K/min. The temperatures of the invariant reactions were determined from the onset. Data for the phase transition temperatures were taken from the heating curves. The liquidus temperatures on heating were evaluated from the peak maximum. In general, no pronounced supercooling effects were observed for the most investigated alloys and the liquidus temperatures for some alloys were therefore taken from the corresponding cooling curves.

3.4. X-ray diffraction analysis

X-ray diffraction (XRD) analysis was carried out to determine the phases present in the alloys, using CuK_α-filtered radiation on powder experimental samples. The fine powder was prepared by grinding in an agate mortar. XRD measurements were performed on a multipurpose X-ray diffractometer Bruker-AXS D8 Discover, Germany operated in Bragg-Brentano reflecting geometry. A fast one dimensional LynxEye detector and a variable slit system with 12 mm illumination length on the sample carrier was used for data

Table 1
The chemical composition of the phases of the La−Ni alloys according to EMPA.

#	Alloy composition, at.%				Heat-treatment	Solidification path/phase composition	EPMA data, at.%		
	nominal		measured				Phase	La	Ni
	La	Ni	La	Ni					
1	7.5	92.5	7.7	92.3	as-cast	L → $(Ni)^a$ → eutectic $((Ni) + LaNi_5)$	(Ni)	0.0 ± 0.0	100.0 ± 0.0
							$LaNi_5$	17.0 ± 0.3	83.0 ± 0.3
							eutectic $((Ni) + LaNi_5)$	9.8	90.2
								9.9	90.1
								8.9	91.1
2	8.5	91.5	9.0	91.0	as-cast	L → eutectic $((Ni) + LaNi_5)$	eutectic $((Ni) + LaNi_5)$	9.0	91.0
								9.2	90.8
								9.1	90.9
								8.8	91.2
3	12.5	87.5	12.5	87.5	as-cast	L → $LaNi_5$ → eutectic $((Ni) + LaNi_5)$	$LaNi_5$	17.0 ± 0.1	83.0 ± 0.1
							(Ni)	0.1 ± 0.1	99.9 ± 0.1
							eutectic $((Ni) + LaNi_5)$	8.5	91.5
								8.7	91.3
4	16	84	16.3	83.7	as-cast	L → $LaNi_5$	$LaNi_5$	16.5 ± 0.1	83.5 ± 0.1
			-	-	1250 °C, 2 h	$LaNi_5$	—	—	—
5	17	83	17.2	82.8	as-cast	L → $LaNi_5$ → La_5Ni_{19} → La_2Ni_7	$LaNi_5$	17.7 ± 0.1	82.3
							La_5Ni_{19}	22.0	78.0
							La_2Ni_7	23.1 ± 0.1	76.9 ± 0.1
6	18	82	−	−	as-cast	L → $LaNi_5$ → La_5Ni_{19} → La_2Ni_7	−	−	−
7	19	81	19.3	80.7	as-cast	L → $LaNi_5$ → La_5Ni_{19} → La_2Ni_7 → $LaNi_3$	$LaNi_5$	17.8 ± 0.1	82.2 ± 0.1
							La_5Ni_{19}	21.9 ± 0.1	78.1 ± 0.1
							La_2Ni_7	23.1 ± 0.3	76.9 ± 0.3
							$LaNi_3$	26.4 ± 0.7	73.6 ± 0.7
8	20	80	20.3	79.7	as-cast	L → $LaNi_5$ → La_5Ni_{19} → La_2Ni_7 → $LaNi_3$	$LaNi_5$	17.7 ± 0.1	82.3 ± 0.1
							La_5Ni_{19}	21.9 ± 0.2	78.1 ± 0.2
							La_2Ni_7	23.3 ± 0.2	76.7 ± 0.2
							$LaNi_3$	25.8 ± 0.3	74.2 ± 0.3
9	24	76	24.1	75.9	as-cast	L → $LaNi_5$ → La_5Ni_{19} → La_2Ni_7 → $LaNi_3$ → La_7Ni_{16}	$LaNi_5$	17.9 ± 0.2	82.1 ± 0.2
							La_5Ni_{19}	21.6	78.4
							La_2Ni_7	23.7 ± 0.1	76.3 ± 0.1
							$LaNi_3$	26.7 ± 0.2	73.3 ± 0.2
							La_7Ni_{16}	32.2 ± 0.3	67.8 ± 0.3
			24.2	75.8	650 °C, 100 h	$La_2Ni_7 + LaNi_3$	La_2Ni_7	23.8 ± 0.1	76.2 ± 0.1
							$LaNi_3$	26.6 ± 0.1	73.4 ± 0.1
10	26.5	73.5	26.9	73.1	as-cast	L → $LaNi_5$ → La_5Ni_{19} → La_2Ni_7 → $LaNi_3$ → La_7Ni_{16} → La_2Ni_3	$LaNi_5$	17.9	82.1
							La_5Ni_{19}	21.7	78.3
							La_2Ni_7	23.8 ± 0.1	76.2 ± 0.1
							$LaNi_3$	26.7 ± 0.2	73.3 ± 0.2
							La_7Ni_{16}	32.6 ± 0.3	67.4 ± 0.3
							La_2Ni_3	41.6 ± 0.2	58.4 ± 0.2
			26.9	73.1	650 °C, 100 h	$LaNi_3 + La_7Ni_{16}$	$LaNi_3$	26.7 ± 0.1	73.3 ± 0.1
							La_7Ni_{16}	32.0 ± 0.1	68.0 ± 0.1
			26.8	73.2	695 °C, 10 h	$LaNi_3 + La_7Ni_{16}$	$LaNi_3$	26.5 ± 0.1	73.5 ± 0.1
							La_7Ni_{16}	32.5 ± 0.1	67.5 ± 0.1
11	29	71	29.2	70.8	as-cast	L → $LaNi_5$ → La_5Ni_{19} → La_2Ni_7 → $LaNi_3$ → La_7Ni_{16} → La_2Ni_3	$LaNi_5$	17.7 ± 0.1	82.3 ± 0.1
							La_2Ni_7	23.6 ± 0.1	76.4 ± 0.1
							$LaNi_3$	26.2 ± 0.2	73.8 ± 0.2
							La_7Ni_{16}	31.5 ± 0.1	68.5 ± 0.1
							La_2Ni_3	41.2 ± 0.1	58.8 ± 0.1
			29.1	70.9	650 °C, 100 h	$LaNi_3 + La_7Ni_{16}$	$LaNi_3$	26.6 ± 0.1	$73.4 \pm 0.$
							La_7Ni_{16}	32.1 ± 0.1	67.9 ± 0.1
			29.2	70.8	695 °C, 10 h	$LaNi_3 + La_7Ni_{16}$	$LaNi_3$	26.5 ± 0.1	$73.5 \pm 0.$
							La_7Ni_{16}	31.9 ± 0.1	68.1 ± 0.1
12	32	68	32.2	67.8	as-cast	L → $LaNi_5$ → La_5Ni_{19} → La_2Ni_7 → $LaNi_3$ → La_7Ni_{16} → La_2Ni_3	$LaNi_5$	17.6 ± 0.3	82.4 ± 0.3
							La_2Ni_7	23.6 ± 0.5	76.4 ± 0.5
							$LaNi_3$	26.7 ± 0.2	73.3 ± 0.2
							La_7Ni_{16}	32.7 ± 0.3	67.3 ± 0.3
							La_2Ni_3	41.8 ± 0.2	58.2 ± 0.2
			32.2	67.8	650 °C, 100 h	$La_7Ni_{16} + La_2Ni_3$	La_7Ni_{16}	32.2 ± 0.3	67.8 ± 0.3
							La_2Ni_3	41.7 ± 0.2	58.3 ± 0.2
13	34	66	34.2	65.8	as-cast	L → $LaNi_5$ → La_5Ni_{19} → La_2Ni_7 → $LaNi_3$ → La_7Ni_{16} → La_2Ni_3 → eutectic $(LaNi + La_2Ni_3)$	La_2Ni_7	23.4 ± 0.1	76.6 ± 0.1
							$LaNi_3$	26.3 ± 0.1	73.7 ± 0.1
							La_7Ni_{16}	31.8 ± 0.4	68.2 ± 0.4
							La_2Ni_3	40.9 ± 0.5	59.1 ± 0.5
							$LaNi$	50.5 ± 0.3	49.5 ± 0.3
			34.2	65.8	650 °C, 100 h	$La_7Ni_{16} + La_2Ni_3$	La_7Ni_{16}	32.2 ± 0.1	67.8 ± 0.1
							La_2Ni_3	41.8 ± 0.2	58.2 ± 0.2
			34.1	65.9	670 °C, 20 h	$La_7Ni_{16} + La_2Ni_3$	La_7Ni_{16}	32.3 ± 0.1	67.7 ± 0.1
							La_2Ni_3	41.8 ± 0.1	58.2 ± 0.1

Table 1 (*continued*)

#	Alloy composition, at.%				Heat-treatment	Solidification path/phase composition	EPMA data, at.%		
	nominal		measured				Phase	La	Ni
	La	Ni	La	Ni					
14	37	63	37.3	62.7	as-cast	L → **La$_2$Ni$_7$** → LaNi$_3$ → La$_7$Ni$_{16}$ → La$_2$Ni$_3$ → eutectic (LaNi + La$_2$Ni$_3$)	La$_2$Ni$_7$	23.8 ± 0.1	76.2 ± 0.1
							LaNi$_3$	26.2 ± 0.2	73.8 ± 0.2
							La$_7$Ni$_{16}$	32.9 ± 0.1	67.1 ± 0.1
							La$_2$Ni$_3$	41.5 ± 0.3	58.5 ± 0.3
							LaNi	50.7 ± 0.4	49.3 ± 0.4
15	43	57	43.1	56.9	as-cast	L → **La$_2$Ni$_3$** → eutectic (LaNi + La$_2$Ni$_3$)	La$_2$Ni$_3$	41.6 ± 0.1	58.4 ± 0.1
							LaNi	51.1 ± 0.3	48.9 ± 0.3
							eutectic (LaNi + La$_2$Ni$_3$)	45.6	54.4
16	45	55	45.6	54.4	as-cast	L → eutectic (LaNi + La$_2$Ni$_3$)	La$_2$Ni$_3$	41.8 ± 0.1	58.2 ± 0.1
							LaNi	51.5	48.5
							eutectic (LaNi + La$_2$Ni$_3$)	45.5	54.5
								45.6	54.4
								45.7	54.3
			45.5	54.5	650 °C, 100 h	LaNi + La$_2$Ni$_3$	La$_2$Ni$_3$	41.6 ± 0.1	58.4 ± 0.1
							LaNi	51.7 ± 0.1	48.3 ± 0.1
17	46	54	46.3	53.7	as-cast	L → **LaNi** → La$_2$Ni$_3$ → eutectic (LaNi + La$_2$Ni$_3$)	La$_2$Ni$_3$	41.6 ± 0.2	58.4 ± 0.2
							LaNi	51.1 ± 0.2	48.9 ± 0.2
							eutectic (LaNi + La$_2$Ni$_3$)	45.5	54.5
								45.7	54.3
			46.5	53.5	650 °C, 100 h	LaNi + La$_2$Ni$_3$	La$_2$Ni$_3$	41.7 ± 0.2	58.3 ± 0.1
							LaNi	51.5 ± 0.2	48.5 ± 0.2
18	65	35	65.4	34.6	as-cast	L → **LaNi** → eutectic (LaNi + La$_7$Ni$_3$)	LaNi	51.5 ± 0.2	48.5 ± 0.2
							eutectic (LaNi + La$_7$Ni$_3$)	65.5	34.5
								65.7	34.3
								65.6	34.4
19	71	29	71.2	28.8	as-cast	L → **La$_7$Ni$_3$**	La$_7$Ni$_3$	71.5 ± 0.4	28.5 ± 0.4
20	73	27	73.6	26.4	as-cast	L → **La$_7$Ni$_3$** → La$_3$Ni	La$_7$Ni$_3$	71.7 ± 0.2	28.3 ± 0.2
							La$_3$Ni	76.0 ± 0.2	24.0 ± 0.2
21	74.5	25.5	74.6	25.4	as-cast	L → **La$_7$Ni$_3$** → La$_3$Ni → eutectic (La$_3$Ni + La$_7$Ni$_3$)	La$_7$Ni$_3$	71.8 ± 0.2	28.2 ± 0.2
							La$_3$Ni	76.5 ± 0.2	23.5 ± 0.2
							eutectic (La$_3$Ni + La$_7$Ni$_3$)	74.6	25.4
22	77	23	77.0	23.0	as-cast	L → eutectic ((βLa) + La$_3$Ni)	(βLa)	100.0 ± 0.0	0.0 ± 0.0
							La$_3$Ni	76.2 ± 0.2	23.8 ± 0.2
							eutectic ((βLa) + La$_3$Ni)	77.5	22.5
								77.1	22.9
								76.8	23.2
								76.5	23.5
23	86	14	86.2	13.8	as-cast	L → **(βLa)** → La$_3$Ni	(βLa)	100.0 ± 0.0	0.0 ± 0.0
							La$_3$Ni	76.6 ± 0.2	23.4 ± 0.2
24	80	20	79.6	20.4	as-cast	L → **(βLa)**[a] → La$_3$Ni	(βLa)	100.0 ± 0.0	0.0 ± 0.0
							La$_3$Ni	76.1 ± 0.3	23.9 ± 0.3

[a] Primary phase is shown in bold.

collection. The lattice parameters were refined by the least-squares method. The phases were determined by comparing the diffraction patterns with the literature or a calculated pattern using the PowderCell [38] and WINXPOW [39] software packages. Both the PowderCell and WINXPOW software packages were used to calculate lattice parameters based on the least-squares method.

4. Experimental investigation

4.1. Binary La−Ni system

Reinvestigation of the binary La−Ni system was needed due to existing contradictions in the literature data for this phase diagram. The La−Ni system was studied in the whole concentration region basing on information from as-cast and annealed alloys of 24 different compositions. The investigation was carried out by DTA, XRD, SEM and EPMA.

Fig. 1 *a* and *b* show the DTA curves of the as-cast alloys 8.5La-91.5Ni and 16La−84Ni indicating the thermal events at 1271 and 1361 °C upon heating for the eutectic reaction L ⇄ (Ni) + LaNi$_5$ and the melting point of LaNi$_5$, respectively. The results obtained are shown in Tables 1 and 2. These two temperatures are in a very good agreement with those reported (1270 and 1350 °C) by Buschow and Mal [19] and (1267 and 1357 °C) by Ivanchenko et al. [20] and less with those reported by Dischinger and Schaller [22] (1279 and 1393 °C). Large effect of supercooling was observed on the cooling curves of these alloys. According to SEM, alloy 8.5La-91.5Ni (Fig. 2 *a*) is completely eutectic ((Ni) + LaNi$_5$), while alloy 16La−84Ni is a completely single phase LaNi$_5$. The eutectic composition according to EPMA data is 9 at.% La (Table 1), which is in good agreement with [19,20,22,25].

As noted in Section 2, Dischinger and Schaller [22] reported a new binary compound La$_4$Ni$_{17}$, which was not found in any other works. In order to confirm or disapprove the presence of this phase, the samples 18La−82Ni, 19La−81Ni and 20La−80Ni were prepared. The microstructure of the as-cast sample 20La−80Ni is shown in Fig. 2 *b*. The solidification path in this alloy is following: after the primary solidification of the LaNi$_5$ phase, the phases La$_5$Ni$_{19}$, La$_2$Ni$_7$ and LaNi$_3$ form through the sequence of peritectic reactions. The phase with composition "La$_4$Ni$_{17}$" was not observed. The DTA curve of this alloy in the as-cast state shows the thermal effects at 1005 and 967 °C corresponding to the peritectic reactions of the

Table 2
Temperatures of phase transformations in the La−Ni system.

#	La	Ni	Liquidus	$L \rightleftarrows (Ni) + LaNi_5$	$L + LaNi_5 \rightleftarrows La_5Ni_{19}$	$L + La_5Ni_{19} \rightleftarrows La_2Ni_7$	$L + La_2Ni_7 \rightleftarrows LaNi_3$	$L + LaNi_3 \rightleftarrows La_7Ni_{16}$	$L + La_7Ni_{16} \rightleftarrows La_2Ni_3$	$L \rightleftarrows LaNi + La_2Ni_3$	$L \rightleftarrows LaNi + La_7Ni_3$	$L \rightleftarrows La_3Ni + La_7Ni_3$	$L \rightleftarrows (\beta La) + La_3Ni$	Others
1	7.5	92.5	$1307\downarrow$[a]	1270	–	–	–	–	–	–	–	–	–	–
2	8.5	91.5	–	1271	–	–	–	–	–	–	–	–	–	–
3	12.5	87.5	1329	1272	–	–	–	–	–	–	–	–	–	–
4	16	84	–	–	–	–	–	–	–	–	–	–	–	*1361* melting temperature of $LaNi_5$; 1301 $L + LaNi_5/LaNi_5$; 1245 $LaNi_5/LaNi_5 + (Ni)$
5	17	83	1359	–	1005	–	–	–	–	–	–	–	–	1312 $L + LaNi_5/LaNi_5$; 1265 $LaNi_5/LaNi_5 + (Ni)$
6	18	82	1364	–	1004	–	–	–	–	–	–	–	–	–
7	19	81	1358	–	1004	–	–	–	–	–	–	–	–	–
8	20	80	1355	–	1005	967	–	–	–	–	–	–	–	–
9	24	76	1326	–	1006 *1006*[b]	968 *967*	792 *793*	702	–	–	–	–	–	–
10	26.5	73.5	1281	–	1008	969	795	699	–	–	–	–	–	581
11	29	71	1220	–	1009 *1009*	969 *970*	797 *797*	696 *696*	673	–	–	–	–	746↓; 754↓; 581
12	32	68	$1125\downarrow$	–	1008 *1008*	969 *967*	796 *797*	695 *694*	673 *672*	659	–	–	–	749↓; 747↓; 581
13	34	66	$1056\downarrow$	–	1010	967 *967*	799 *797*	700 *701*	676 *674*	659	–	–	–	728↓; 725↓; 580
14	37	63	$934\downarrow$	–	–	–	798	702	673	660	–	–	–	722↓; 581
15	43	58	673	–	–	–	–	–	–	655	–	–	–	–
16	45	55	$658\downarrow$	–	–	–	–	–	–	658	–	–	–	–
17	46	54	$665\downarrow$	–	–	–	–	–	–	655 *658*	–	–	–	–
18	65	35	542	–	–	–	–	–	–	–	523	–	–	–
19	71	29	–	–	–	–	–	–	–	–	–	–	–	541 melting temperature of La_7Ni_3
20	73	27	$538\downarrow$	–	–	–	–	–	–	–	–	534	–	–
21	74.5	25.5	$536\downarrow$	–	–	–	–	–	–	–	–	534	–	–
22	77	23	$635\downarrow$	–	–	–	–	–	–	–	–	–	531	–
23	80	20	594	–	–	–	–	–	–	–	–	–	530	–
24	86	14	708	–	–	–	–	–	–	–	–	–	532	–
Average[c]				1271 ± 1	1007 ± 3	968 ± 2	796 ± 3	698 ± 4	674 ± 2	658 ± 3	523	534 ± 1	531 ± 1	–

[a] ↓ − DTA data on cooling.
[b] In *italic* on annealed alloys.
[c] Mean-square deviations.

formation of the La_5Ni_{19} and La_2Ni_7 phases, respectively, which is in good agreement with Yamamoto et al. [30] and An et al. [25], where the temperature of the formation of the La_5Ni_{19} phase ($L + LaNi_5 \rightleftarrows La_5Ni_{19}$) was reported to be ~1000 and 1003 °C, respectively. It should be noted that in the works [19–22] the phase La_5Ni_{19} was not found, so for the region between $LaNi_5$ and La_2Ni_7 a temperature of 995 °C [19] (1007 °C [20], 1014 [21] and 1019 °C [22]) was reported, for what was believed to be the peritectic reaction $L + LaNi_5 \rightleftarrows La_2Ni_7$, and a temperature of 955 °C [19] (967 °C [20]) for the peritectic reaction $L + La_2Ni_7 \rightleftarrows LaNi_3$ or polymorphic transformation of La_2Ni_7 (976 °C [21]). In addition to that, according to Yamamoto et al. [30] the La_5Ni_{19} phase decomposes into La_2Ni_7 and $LaNi_5$ phases at a temperature between 900 and 1000 °C, while according to the thermodynamic modeling of An et al. [25] this phase is stable at low temperatures. According to our data this phase is stable at least up to 600 °C.

Fig. 1 c shows the DTA result of as-cast 26.5La-73.5Ni alloy upon heating up to 1320 °C indicating five thermal events. The cooling curve also shows these transformations with some slight supercooling. As noted above, thermal effects at 1008 and 969 °C (Table 2) correspond to the peritectic reactions $L + LaNi_5 \rightleftarrows La_5Ni_{19}$ and $L + La_5Ni_{19} \rightleftarrows La_2Ni_7$, respectively, which is in a good agreement with An et al. [25]. The thermal effects at 795 and 699°C correspond to the peritectic reactions $L + La_2Ni_7 \rightleftarrows LaNi_3$ and $L + LaNi_3 \rightleftarrows La_7Ni_{16}$, which is somewhat lower than proposed in the works [21,22,25]. The small DTA effect at 581 °C, which was not previously observed, possibly corresponds to the polymorphic transformation or eutectic decomposition of the La_7Ni_{16} (or La_2Ni_3) phase. It should be noted that this effect at 581 °C was not observed on DTA curve of the annealed alloy. The solidification path in this alloy and in the alloy 29La−71Ni is rather complex: after the primary solidification of the $LaNi_5$ phase, the phases La_5Ni_{19}, La_2Ni_7, $LaNi_3$, La_7Ni_{16} and La_2Ni_3 form through the sequence of peritectic reactions (Table 1). The X-ray diffraction pattern of the as-cast sample 29La−71Ni is shown in Fig. 3, which confirms the presence of phases $LaNi_5$, La_2Ni_7, $LaNi_3$, La_7Ni_{16} and La_2Ni_3 (Table 3). Only the La_5Ni_{19} phase was not observed in the X-ray diffraction pattern of this alloy, probably due to its very small amount. After annealing at 650 °C/100 h the 24La−76Ni alloy has a two-phase structure: $LaNi_3$ + La_2Ni_7 (Fig. 4 a, Table 1), while the alloys 26.5La-73.5Ni and 29La−71Ni annealed at 650 °C/100 h and at subsolidus temperature (695 °C/10 h) are two-phase $LaNi_3$ + La_7Ni_{16} (Fig. 4 b, Table 1).

Fig. 1 d shows the DTA result of the 32La−68Ni alloy in as-cast
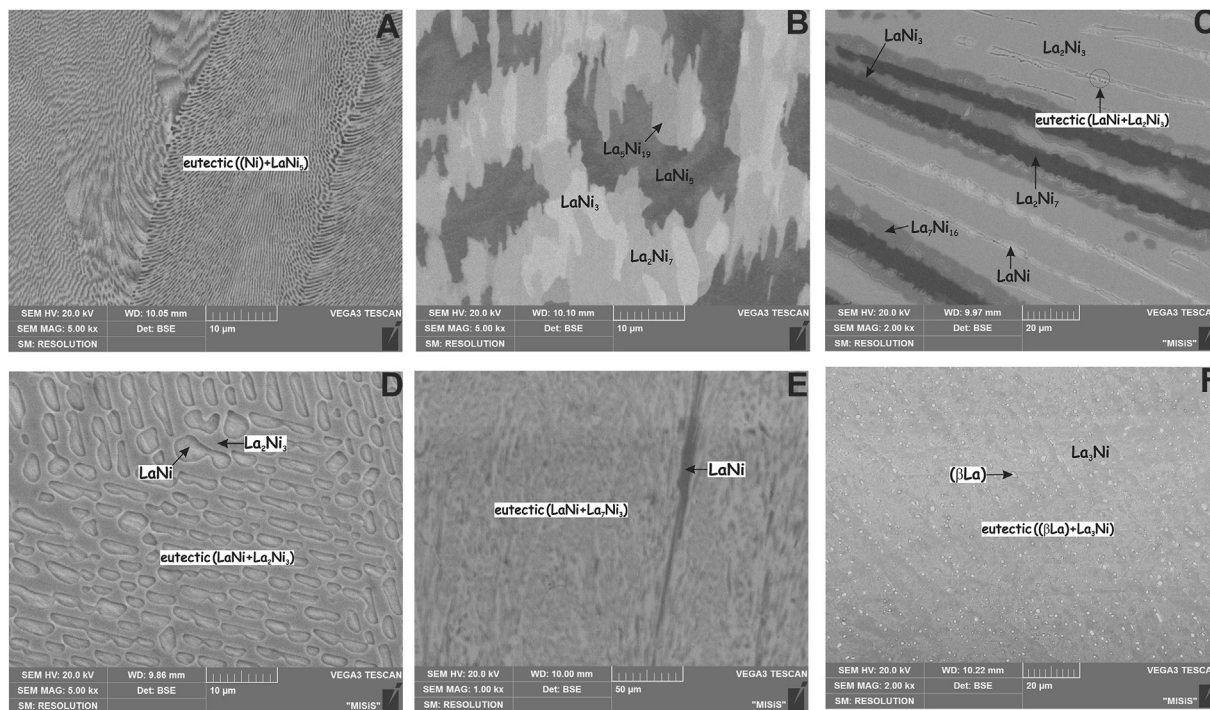
Fig. 2. Microstructure of as-cast alloys of the La−Ni system:
a − 8.5La-91.5Ni, × 5000, eutectic ((Ni) + LaNi$_5$);
b − 20La−80Ni, × 5000, LaNi$_5$ + La$_5$Ni$_{19}$ + La$_2$Ni$_7$ + LaNi$_3$;
c − 37La−63Ni, × 2000, La$_2$Ni$_7$ + LaNi$_3$ + La$_7$Ni$_{16}$ + La$_2$Ni$_3$ + eutectic (LaNi + La$_2$Ni$_3$);
d − 45La−55Ni, × 5000, eutectic (LaNi + La$_2$Ni$_3$);
e − 65La−35Ni, × 1000, LaNi + eutectic (LaNi + La$_7$Ni$_3$);
f − 77La−23Ni, × 2000, eutectic ((βLa) + La$_3$Ni).
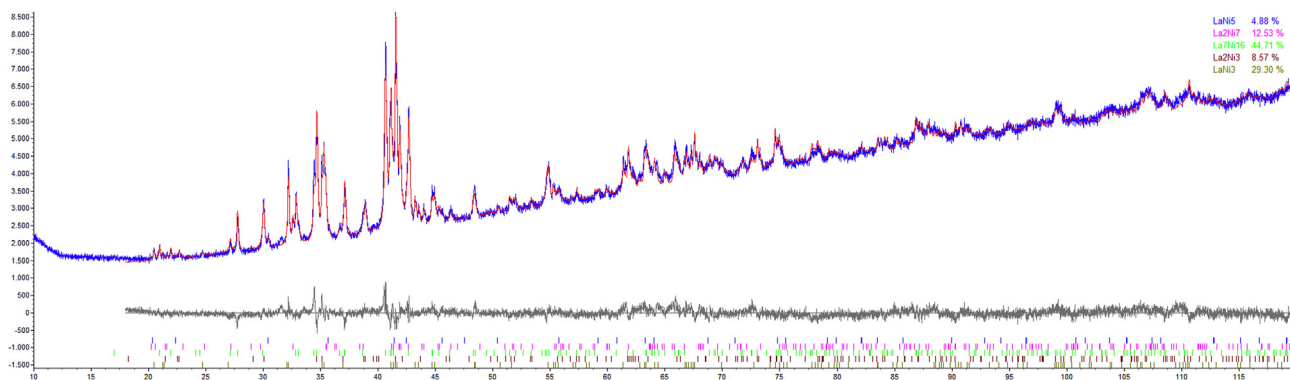
Fig. 3. X-ray diffraction pattern of the as-cast alloy 29La−71Ni. Red curve: pattern calculated from Rietveld Refinement; blue curve: experimental pattern; grey curve, bottom: difference curve.

state. As noted above, the temperatures 1008, 969, 796 and 696 °C correspond to the peritectic reactions L + LaNi$_5$ ⇄ La$_5$Ni$_{19}$, L + La$_5$Ni$_{19}$ ⇄ La$_2$Ni$_7$, L + La$_2$Ni$_7$ ⇄ LaNi$_3$ and L + LaNi$_3$ ⇄ La$_7$Ni$_{16}$, respectively. The thermal effect at 672°C corresponds to the peritectic reaction L + La$_7$Ni$_{16}$ ⇄ La$_2$Ni$_3$, which is lower than reported early (688 °C [21,25], 690 °C [19] and 701 °C [22]). It should be noted that on the DTA curve of this alloy, as well as of some other alloys, double thermal arrests at 1006 and at 969 °C were observed both for as-cast and annealed alloys. These effects can be associated with polymorphic transformations of the La$_5$Ni$_{19}$ and La$_2$Ni$_7$ phases. The small DTA effect at 581 °C is also observed. In addition, on the cooling curve of this alloy, as well as on the curves of alloys 29La−71Ni, 34La−66Ni and 37La−63Ni, the thermal effect at

~730 °C was observed. The nature of this effect is not known. SEM micrographs of alloys 32La−68Ni and 34La−66Ni in as-cast state show primarily solidified LaNi5 phase, and then the phases La$_5$Ni$_{19}$, La$_2$Ni$_7$, LaNi$_3$, La$_7$Ni$_{16}$ and La$_2$Ni$_3$ crystallize and the solidification finishes with the formation of the small amount of eutectic (LaNi + La$_2$Ni$_3$). In the as-cast alloy 37La−63Ni (Fig. 2 c, Table 1) the LaNi$_5$ and La$_5$Ni$_{19}$ phases were not observed, the La$_2$Ni$_7$ phase is the primary, and then the phases LaNi$_3$, La$_7$Ni$_{16}$ and La$_2$Ni$_3$ crystallize and the solidification finishes with the formation of the eutectic (LaNi + La$_2$Ni$_3$). After annealing at 650 °C/100 h the alloys 32La−68Ni and 34La−66Ni are two-phase La$_2$Ni$_3$ + La$_7$Ni$_{16}$ (Fig. 4 c, Table 1).

As it was noted in Section 2, the temperatures of eutectics in the

Table 3
The crystal structure and lattice parameters of the La−Ni−Fe phases.

| Phase	Crystal structure	Lattice parameters, Å	Remarks	Ref.
(δFe)	W, cI2-Im-3m	$a = 2.9315$	at >1394 °C	[40]
(γFe)	Cu, cF4-Fm-3m	$a = 3.6467$	at >912 °C	[40]
		$a = 3.581(1)$	25Fe−55Ni−20La, as-cast	Th.w.
(αFe)	W, cI2-Im-3m	$a = 2.8665$	at 25 °C	[40]
		$a = 2.865(1)$	5Fe−45Ni−50La, as-cast	Th.w.
(εFe)	Mg, hP2-P6₃/mmc	$a = 2.468, c = 3.96$	at 25 °C, >13 GPa	[40]
(γLa)	W, cI2-Im-3m	$a = 4.26$	at >865 °C	[40]
(βLa)	Cu, cF4-Fm-3m	$a = 5.303$	at >310 °C	[40]
(αLa)	αLa, hP4-P6₃/mmc	$a = 3.7740, c = 12.171$	at 25 °C	[40]
(Ni)	Cu, cF4-Fm-3m	$a = 3.5240$	at >25 °C	[40]
LaNi₅	CaCu₆, hP6-P6/mmm	$a = 5.017, c = 3.987$	–	[19]
		$a = 5.03286(93), c = 3.9764(13)$	29La−71Ni, as-cast	Th.w.
		$a = 5.056(2), c = 4.021(3)$	30Fe−55Ni−15La, as-cast	Th.w.
		$a = 5.065(1), c = 4.023(1)$	25Fe−55Ni−20La, as-cast	Th.w.
La₅Ni₁₉	Ce₅Co₁₉, hR72-R-3m	-	–	[30]
	Pr₅Co₁₉ (Sm₅Co₁₉), hP48-P6₃/mmc	$a = 5.0491(1), c = 32.642(1)$	–	[32]
		$a = 5.0518(8), c = 32.652(5)$	–	[25]
βLa₂Ni₇	Gd₂Co₇, hR54-R-3m	$a = 5.056, c = 36.98$	as-cast	[27]
αLa₂Ni₇	Ce₂Ni₇, hP36-P6₃/mmc	$a = 5.053, c = 24.62$	at 800 °C	[27]
		$a = 5.058, c = 24.71$	–	[19]
		$a = 5.06237(20), c = 24.6864(22)$	29La−71Ni, as-cast	Th.w.
		$a = 5.092(2), c = 24.843(8)$	30Fe−55Ni−15La, as-cast	Th.w.
LaNi₃	PuNi₃, hR36-R-3m	$a = 5.086, c = 25.01$	at 600 °C	[27]
		$a = 5.083, c = 25.09$	–	[19]
La₂Ni₃	La₂Ni₃, oS20-Cmca	$a = 5.1138, b = 9.7316,$ $c = 7.9075$	–	[28]
		$a = 5.117(2), b = 9.746(3),$ $c = 7.907(2)$	25Fe−55Ni−20La, as-cast	Th.w.
		$a = 5.10690(58), b = 9.72343(98), c = 7.89528(76)$	29La−71Ni, as-cast	Th.w.
La₇Ni₁₆	La₇Ni₁₆, tI46-I-42 m	$a = 7.355, c = 14.51$	–	[41]
		$a = 7.36870(18), c = 14.5485(53)$	29La−71Ni, as-cast	Th.w.
LaNi	CrB, oS8-Cmcm	$a = 3.907(1), b = 10.810(1),$ $c = 4.396(1)$	–	[42]
		$a = 3.91, b = 10.80, c = 4.39$	–	[19]
		$a = 3.920(3), b = 10.820(8),$ $c = 4.403(1)$	5Fe−45Ni−50La, as-cast	Th.w.
La₇Ni₃	Fe₃Th₇, hP20-P6₃/mc	$a = 10.14, c = 6.383$	–	[43]
		$a = 10.140(5), c = 6.475(3)$	–	[44]
		$a = 10.204(3), c = 6.391(2)$	5Fe−45Ni−50La, as-cast	Th.w.
La₃Ni	Fe₃C, oP16-Pnma	$a = 7.22, b = 10.24, c = 6.60$	–	[45]
		$a = 7.271(3), b = 10.243(4),$ $c = 6.647(3)$	–	[46]

Th.w. − the result of this work.

La-rich side of the La−Ni system differ significantly according to various authors. The temperature of the eutectic reaction L ⇄ LaNi + La₂Ni₃ according to the calculation from An et al. [25] and the experimental data from Ivanchenko et al. [20] is 675 °C and 667°C, respectively, while according to the experimental data from Dischinger and Schaller [22] it is much higher i.e. 690°C. Therefore, in order to check the temperature of this reaction, alloys with the compositions 43La−57Ni, 45La−55Ni and 46La−54Ni were prepared. The current measurements indicate that the temperature of this eutectic reaction is 658°C (see Fig. 1 e, Table 2), which is in good agreement with the experimental data from Ivanchenko et al. [20], but is significantly lower than suggested in Ref. [22,25]. The microstructure of 46La−54Ni alloy in as-cast state shows the primary LaNi phase, the La₂Ni₃ phase and the eutectic (LaNi + La₂Ni₃), while in the 43La−57Ni alloy primary crystals of La₂Ni₃ phase and the eutectic (LaNi + La₂Ni₃) can be observed. The alloy 45La−55Ni (Fig. 2 d) is completely eutectic (LaNi + La₂Ni₃). The eutectic composition was determined by EPMA as 45.6 at.% La (Table 1). After annealing at 650 °C/100 h the alloys 45La−55Ni and 46La−54Ni are two-phase La₂Ni₃ + LaNi (Fig. 4 d).

Some controversy can be observed concerning the temperature of the eutectic reaction L ⇄ LaNi + La₇Ni₃. According to the calculation by An et al. [25] the temperature of this reaction is 517°C, whereas according to the experimental data Dischinger and

Schaller [22] it is much higher (560°C). In order to check the temperature of this reaction an alloy 65La−35Ni was prepared. The microstructure of this alloy (Fig. 2 e) shows a small amount of primary LaNi phase and a large amount of eutectic (LaNi + La₇Ni₃). The eutectic temperature was measured to be 523 °C (Fig. 1 f, Table 2), the eutectic composition according to EPMA data is 65.6 at.% La (Table 1). As it can be seen, the eutectic composition and the temperature are in good agreement with calculation An et al. [25] and contradictory to the experimental data of Dischinger and Schaller [22].

The eutectic temperature L ⇄ La₃Ni + La₇Ni₃ was measured only by Dischinger and Schaller [22] as 545°C. However, according to the calculation by An et al. [25] the temperature of this eutectic is noticeably lower and is equal to 530°C. Verification of the temperature for this eutectic was performed on the as-cast samples 71La−29Ni, 73La−27Ni and 74.5La-25.5Ni. The eutectic temperature equal to 534 °C was determined using DTA, as shown in Fig. 1 g, which is in a very good agreement with the thermodynamic evaluation [25] and in contradiction to the results of [22]. It should be noted that the alloy 71La−29Ni, which according to Refs. [25] corresponds to the composition of the eutectic (La₃Ni + La₇Ni₃) is completely single-phase La₇Ni₃. The microstructure of the alloy 73La−27Ni shows the primarily crystallized La₇Ni₃ phase and the La₃Ni phase, while the alloy 74.5La-25.5Ni is completely eutectic
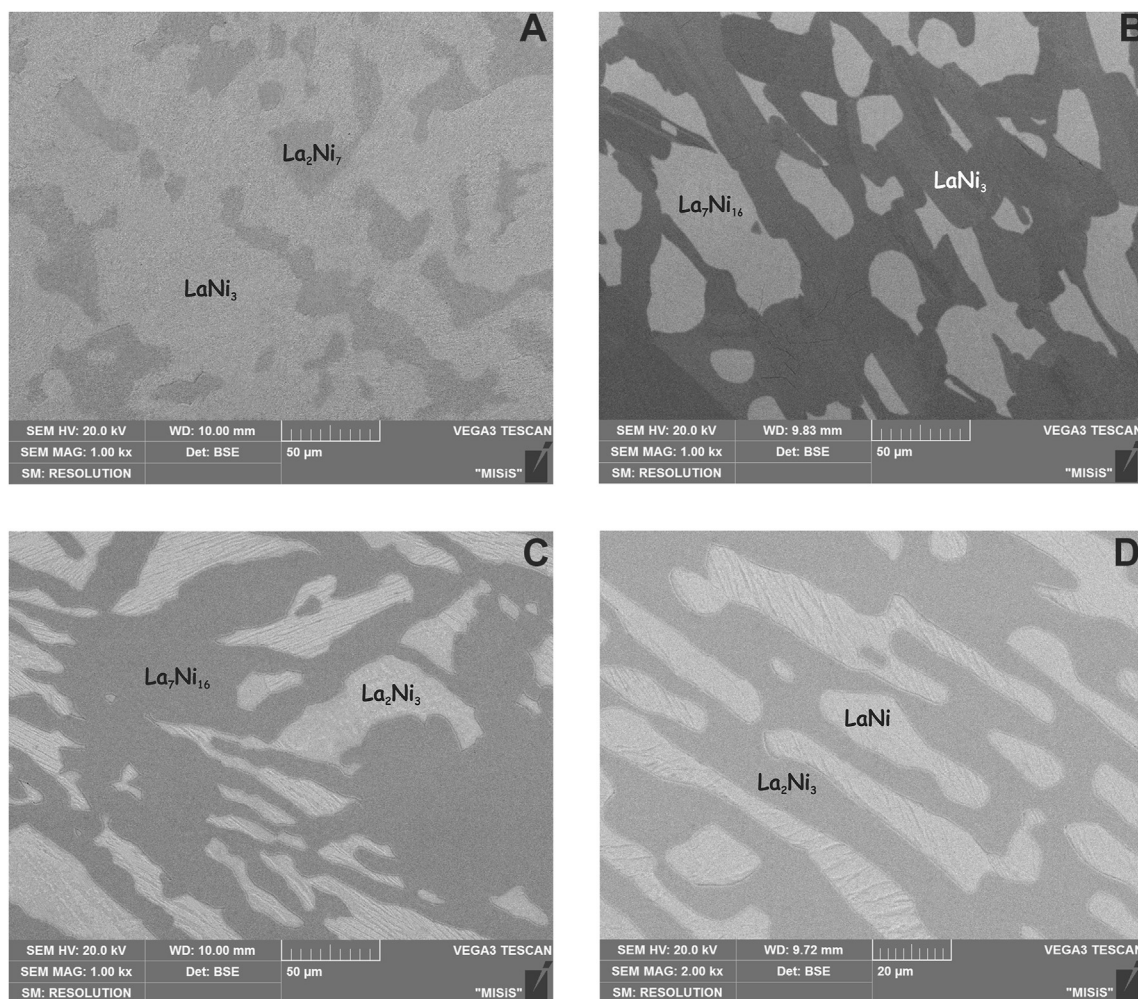
Fig. 4. Microstructure of annealed alloys of La−Ni system:
a − 24La−76Ni, 650 °C/100 h, × 1000, La_2Ni_7 + $LaNi_3$;
b − 26.5La-73.5Ni, 695 °C/10 h, × 1000, $LaNi_3$ + La_7Ni_{16};
c − 34La−66Ni, 650 °C/100 h, × 1000, La_7Ni_{16} + La_2Ni_3;
d − 45La−55Ni, 650 °C/100 h, × 2000, La_2Ni_3 + LaNi.

(La_3Ni + La_7Ni_3). The eutectic composition was determined by EPMA as 74.6 at.% La (Table 1), which is slightly higher than that proposed in Ref. [25].

Some temperature discrepancies were also found for the eutectic reaction L ⇄ (βLa) + La_3Ni. Indeed a temperature of 527°C was measured by Ref. [20], 31 °C higher than those measured by Ref. [18] and 33 °C lower than measured by Ref. [22]. Verification of the temperature for this eutectic was performed on an the as-cast samples 86La−14Ni, 80La−20Ni and 77La−23Ni. The results obtained are shown in Tables 1 and 2 and Fig. 1 *h*, 2 *f*. The microstructure of the alloys 86La−14Ni and 80La−20Ni shows the primary crystals of (βLa)-phase and the eutectic (βLa) + La_3Ni. The microstructure of the alloy 77La−23Ni (Fig. 2 *f*) seems to be completely eutectic (βLa) + La_3Ni. The composition of this eutectic was established by the microprobe method as 77 at.% La, which is lower than suggested in Ref. [20,25], where the composition of the eutectic is defined as 80 and 84 at.% La, respectively. The temperature of this eutectic according to DTA is 531°C (Fig. 1 *h*), which is in good agreement with the experimental data [20], but noticeably lower than that proposed in Ref. [22].

The revised phase diagram of the La−Ni system is shown in Fig. 5. The existence of compounds $LaNi_5$, La_5Ni_{19}, La_2Ni_7, $LaNi_3$,

La_7Ni_{16}, La_2Ni_3, LaNi, La_7Ni_3 and La_3Ni were confirmed by DTA, XRD, SEM and EPMA. The existence of phase with composition "La_4Ni_{17}" [22] was not confirmed. The $LaNi_5$ phase has some homogeneity range, that agrees with [19−21,31], but contradicts to Refs. [22,23,25,34]. The five eutectic reactions L ⇄ (Ni) + $LaNi_5$ at 1271 ± 1 °C and 9 at.% La, L ⇄ LaNi + La_2Ni_3 at 658 ± 3 °C and 45.6 at.% La, L ⇄ LaNi + La_7Ni_3 at 523 °C and 65.6 at.% La, L ⇄ La_3Ni + La_7Ni_3 at 534 ± 1 °C and 74.6 at.% La and L ⇄ (βLa) + La_3Ni at 531 ± 1 °C and 77 at.% La are well established. The solubility of La in Ni is negligible and does not exceed 0.1 at.%. The solubility of Ni in La is absent.

4.2. Ternary La−Ni−Fe system

In order to establish the phase equilibria in the La−Ni−Fe system during solidification, more than 40 samples have been prepared and characterized. Based on the results of this research, liquidus and solidus projections and the melting diagram of the La−Ni−Fe system have been constructed over the whole composition range (Fig. 6). The phase compositions of the studied alloys and composition of the phases according to the microprobe results are presented in Tables 4 and 5 respectively. The annealing
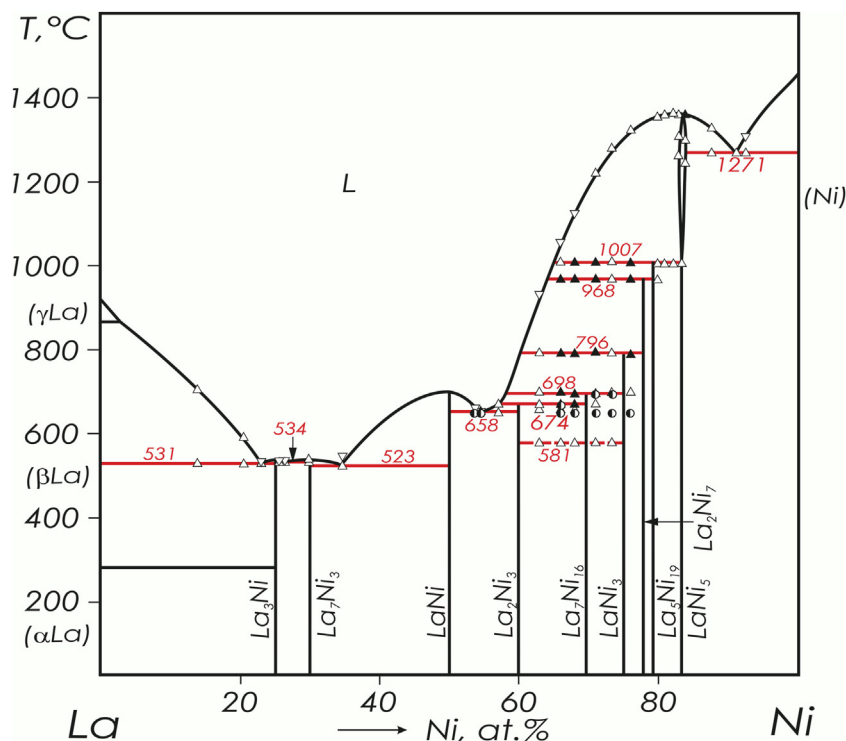
Fig. 5. Phase diagram of La–Ni system: △, ▲ – DTA data of as-cast and annealed alloys, respectively; ◖ – two-phase sample.

temperatures ($T_{ann} = T_{sol} − 5 … 15$ °C) were selected based on the alloys' solidus temperatures as determined from the DTA curves of the as-cast and annealed alloys. The microstructures of some as-cast and annealed samples are shown in Fig. 7 and Fig. 8, respectively.

4.2.1. Solid phases

Some of the phases extend into the ternary system, forming solid-solutions with some changes in their lattice parameters. The extension of these solid solutions and their homogeneity ranges are shown in the solidus projection of the system (Fig. 6 b).

The compounds from the binary La–Ni system containing less than 50 at.% Ni do not dissolve Fe, while those with higher nickel content show large solubility of the third element. Among binary compounds, LaNi$_5$, La$_5$Ni$_{19}$ and La$_2$Ni$_7$ have the largest homogeneity ranges at solidus temperature and according to EPMA data dissolve 21.9, 16.1 and 14.0 at.% Fe, respectively. The homogeneity ranges of the remaining phases are smaller. The solubility of Fe in LaNi$_3$ and La$_2$Ni$_3$ is 2.7 and 2.0 at.%, respectively. The solubility of Fe in LaNi, La$_7$Ni$_{16}$, LaNi, La$_7$Ni$_3$ and La$_3$Ni according to EPMA does not exceed 1 at. %. The maximum solubilities of lanthanum in the (γFe,Ni) and (αFe) phases are defined as less than 1 at.% (Table 5).

The existence of the ternary compound LaNi$_3$Fe$_2$ with a hexagonal structure, which was reported in [36], was not confirmed in our study. It should be noted, that ternary compound was not observed in [35, 37] as well.

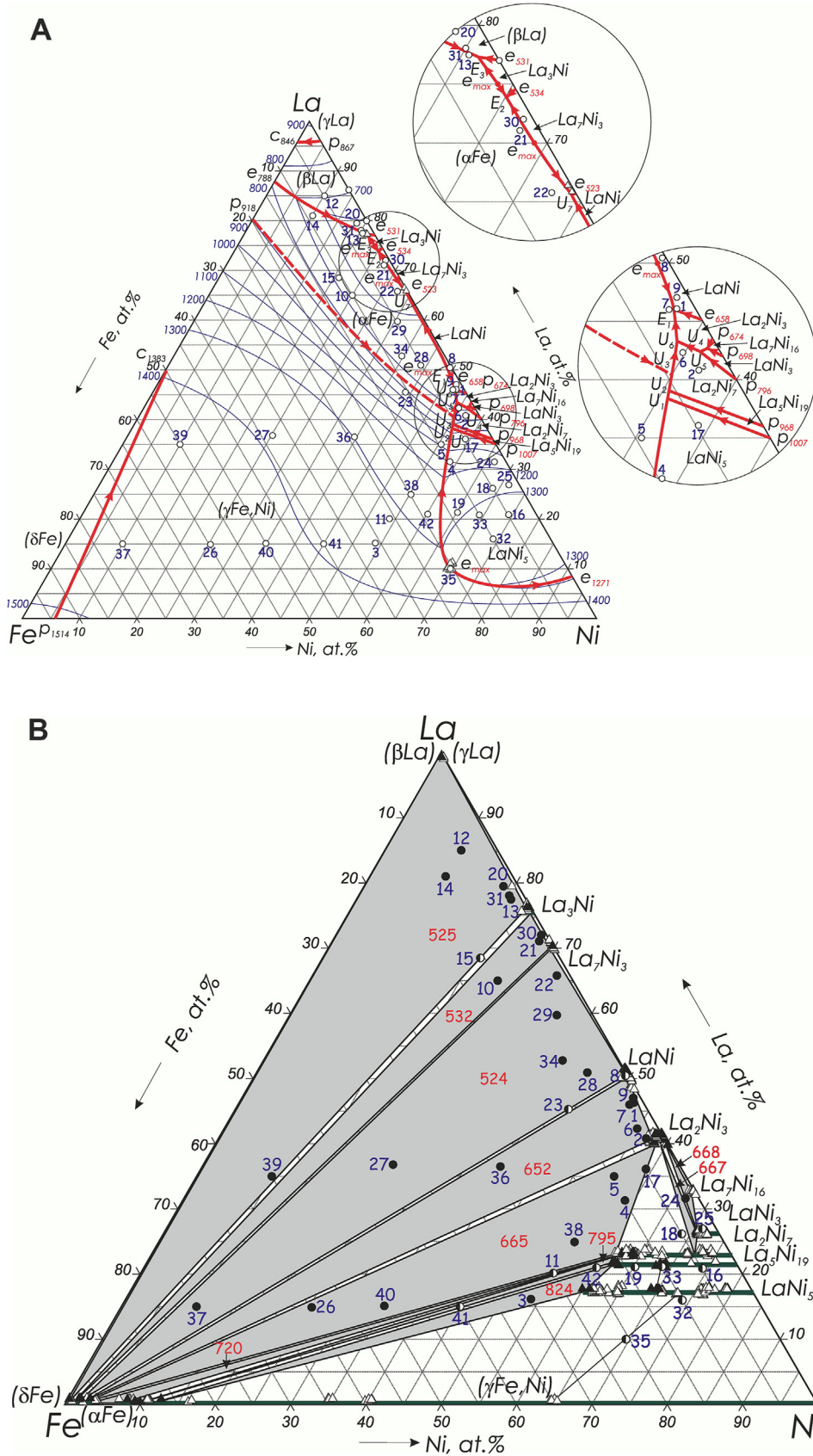### 4.2.2. Liquidus projection

Fig. 6 a shows the liquidus surface projection of the La–Ni–Fe system in the whole composition range resulting from this research. The liquidus surface is characterized by 13 primary solidification fields of the component based solid solutions (γFe,Ni), (δFe), (βLa), (γLa), (αFe) and solid solutions based on binary phases LaNi$_5$, La$_5$Ni$_{19}$, La$_2$Ni$_7$, LaNi$_3$, La$_7$Ni$_{16}$, La$_2$Ni$_3$, LaNi, La$_7$Ni$_3$ and La$_3$Ni, separated by appropriate monovariant curves and participating in

ten four-phase invariant equilibria. Three four-phase invariant equilibria are of the eutectic type, and the remaining are of the transitional type.

The (γFe,Ni) and (αFe) phases define the character of phase equilibria in the La–Ni–Fe system. The fields of their primary crystallization borders with the fields of primary crystallization of most of the phases (δFe), (βLa), LaNi$_5$, La$_5$Ni$_{19}$, La$_2$Ni$_7$, La$_2$Ni$_3$, LaNi, La$_7$Ni$_3$ and La$_3$Ni. The (γFe,Ni)-phase has the widest region of primary crystallization. Noticeably smaller are the regions of LaNi$_5$, (αFe) and (βLa). The remaining phases have very small fields of primary crystallization, and the fields of primary crystallization of LaNi$_3$, La$_7$Ni$_{16}$, La$_2$Ni$_3$, LaNi, La$_7$Ni$_3$ and La$_3$Ni extend parallel to the La–Ni side.

The analysis of the microstructures of the as-cast samples showed that most of the investigated alloys are located in the field of primary crystallization of (γFe,Ni). Typical microstructures of alloys from this region are shown in Fig. 7 a, b. Black primary crystals of this phase are clearly visible on the microstructure. This field is limited by the composition of the alloy #5, which contains only small amount of primary (γFe,Ni)-phase. The microstructure of this alloy is shown in Fig. 7 a. The solidification path in the alloys ## 5, 11, 38, 42 is rather complex: after primary crystallization of the (γFe,Ni) phase, the phases LaNi$_5$, La$_2$Ni$_7$ and La$_2$Ni$_3$ crystallize by peritectic reactions and the solidification finishes with the formation of the LaNi phase (Fig. 7 a). The XRD patterns of these alloys have confirmed the existence of all these phases (Fig. 9). It should be noted, that according to the XRD data, in addition to the (γFe,Ni)-phase, the (αFe)-phase also can be clearly identified in these alloys due to consequent allotropic transformation on cooling (Fig. 9).

The alloys ## 4, 16–19, 24, 25, 32, 33 are located in the field of primary crystallization of the LaNi$_5$ phase (Fig. 7 c-f). The microstructure of alloy # 32 (Fig. 7 c) reveals that the primary phase in this alloy is LaNi$_5$ and then the eutectic (γFe,Ni) + LaNi$_5$ crystallizes with a composition measured by microprobe method as 20Fe–69Ni–11La. The alloy #35 is complete eutectic

Fig. 6. Liquidus (a) and solidus (b) projections and the melting diagram (c) of the La−Ni−Fe system: ○ − composition of sample, ◖ − two-phase sample, ● − three-phase sample, △ and ▲ − EPMA data of as-cast and annealed alloys, respectively.
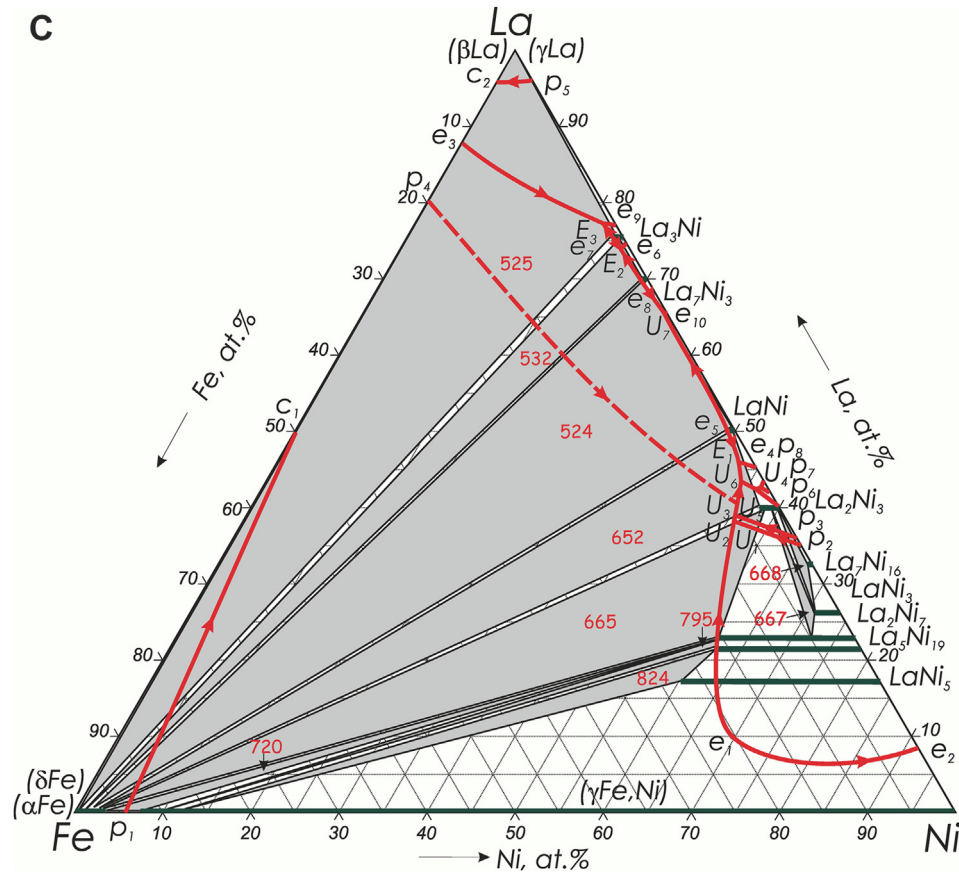
Fig. 6. (continued).

(γFe,Ni) + LaNi$_5$ (Fig. 7 g). Therefore the monovariant curve L $\rightleftarrows$ (γFe,Ni) + LaNi$_5$ ($e_2e_1U_1$), corresponding to joint crystallization of (γFe,Ni) and LaNi$_5$, passes through this composition (see Fig. 6 c). The position of this monovariant curve is also obvious from the observation of the primary (γFe,Ni) phase in samples #5 (Fig. 7 a) and #42 in contrast to the primary LaNi$_5$ phase in samples #4 (Fig. 7 f) and #19. The solidification of alloy #4 (Fig. 7 f) starts with the formation of the LaNi$_5$ phase, followed by the La$_2$Ni$_7$, La$_2$Ni$_3$ and LaNi phases. It should be noted that the equilibrium L + (γFe,Ni) + LaNi$_5$ along the curve $e_2e_1U_1$ changes its character from eutectic L $\rightleftarrows$ (γFe,Ni) + LaNi$_5$ in the La−Ni binary system to peritectic L + (γFe,Ni) $\rightleftarrows$ LaNi$_5$ in the ternary La−Ni−Fe system and this curve ($e_2e_1U_1$) intersects the homogeneity region of the LaNi$_5$ phase (Fig. 6 c).

The alloys ##7, 10, 13−15, 21, 22, 28, 29, 34 are located in the field of primary crystallization of the (αFe)-phase (Fig. 7h−j). The border of this field is limited by the composition of alloys ## 7, 13, 14, 21, 22, in which only a small amount of primary crystals of the (αFe)-phase are observed (Fig. 7h and i).

In the La-rich corner and along the La−Ni side the fields of primary crystallization of phases based on the components (βLa) and (γLa) and phases based on binary compounds La$_5$Ni$_{19}$, La$_2$Ni$_7$, LaNi$_3$, La$_7$Ni$_{16}$, La$_2$Ni$_3$, LaNi, La$_7$Ni$_3$ and La$_3$Ni are present. They are all very small. The fields of (γLa) and (δFe) are shown tentatively. The field (βLa) was plotted basing on the observation of the primary (βLa) phase in alloys ##12, 20 and #31 in contrast to the primary (αFe)-phase in alloys #13 and #14. Moreover, in the last two alloys the amount of primary (αFe)-phase is very small, therefore, the monovariant curve of joint crystallization of the phases (αFe) and (βLa) is located very close to the composition of these alloys. In

alloys #20 and #31 the solidification finishes with the formation of the ternary eutectic (αFe) + (βLa) + La$_3$Ni. The composition of this ternary eutectic according to the EPMA data of these alloys is 1.4Fe-77.3La-21.3Ni (Table 5).

Only the alloys #2 and #6 are located in the field of the primary crystallization of the La$_2$Ni$_7$ phase. The microstructure of the alloy #6 is shown in Fig. 7 k, from which it can be seen that after the primary crystallization of the La$_2$Ni$_7$ phase, the La$_2$Ni$_3$ phase crystallizes in this alloy and solidification finishes with the formation of the eutectic (La$_2$Ni$_3$ + LaNi).

No structures were observed with primary crystallized La$_5$Ni$_{19}$ phase, but it should be noted that the related region is very narrow and is limited by the compositions points of alloys #17 and #2, in which primary are LaNi$_5$ and La$_2$Ni$_7$ phase, respectively. It is worth noting that among the as-cast alloys the La$_5$Ni$_{19}$ phase was observed only in alloys ## 16, 18 and #33. The microstructure of the last alloy (Fig. 7 d) reveals that the primary phase in this alloy is LaNi$_5$, and then the phases La$_5$Ni$_{19}$, La$_2$Ni$_7$ and La$_2$Ni$_3$ form by the peritectic reactions.

Even though, no alloys were located in the fields of primary crystallization of the LaNi$_3$ and La$_7$Ni$_{16}$ phases as well, their position cannot differ substantially from that shown in Fig. 6 a, because these fields are very small and are limited by the compositions points of alloys #2 and #6. The monovariant curves L + La$_2$Ni$_7$ $\rightleftarrows$ LaNi$_3$ (p_6U_5), L + LaNi$_3$ $\rightleftarrows$ La$_7$Ni$_{16}$ (p_7U_4) and L + La$_7$Ni$_{16}$ $\rightleftarrows$ La$_2$Ni$_3$ (p_8U_4) (Fig. 6 c) do not extend appreciably into the ternary system, since in alloys #2 and #6 the La$_2$Ni$_7$ phase is primary, and, moreover, the LaNi$_3$ and La$_7$Ni$_{16}$ phases in these alloys were not observed. The intersection of the monovariant curves L + LaNi$_3$ $\rightleftarrows$ La$_7$Ni$_{16}$ (p_7U_4) and L + La$_7$Ni$_{16}$ $\rightleftarrows$ La$_2$Ni$_3$ (p_8U_4) gives the

Table 4
Phase composition of the studied alloys of the La−Ni−Fe system.

#	Fe	Ni	La	Liquidus temperature, °C	Solidification path	Solidus temperature, °C	Phase composition at solidus surface
1	1.5	52.5	46.0	671	L → **LaNi**[a] → La$_2$Ni$_3$ → eutectic ((αFe) + La$_2$Ni$_3$ + LaNi)	651	(αFe) + La$_2$Ni$_3$ + LaNi
2	3	57	40	698↓[b]	L → **La$_2$Ni$_7$** → La$_2$Ni$_3$ → LaNi	652	(αFe) + La$_2$Ni$_3$ + LaNi
3	30	55	15	1329	L → **(γFe,Ni)** → LaNi$_5$ → La$_2$Ni$_7$ → La$_2$Ni$_3$	824	LaNi$_5$ + (αFe) + La$_2$Ni$_7$
4	10	60	30	1169	L → **LaNi$_5$** → La$_2$Ni$_7$ → La$_2$Ni$_3$ → LaNi	666	La$_2$Ni$_7$ + (αFe) + La$_2$Ni$_3$
5	10	55	35	1092	L → **(γFe,Ni)** → LaNi$_5$ → La$_2$Ni$_7$ → La$_2$Ni$_3$ → LaNi	665	La$_2$Ni$_7$ + (αFe) + La$_2$Ni$_3$
6	5	55	40	681	L → **La$_2$Ni$_7$** → La$_2$Ni$_3$ → LaNi → eutectic (LaNi + La$_2$Ni$_3$)	652	(αFe) + La$_2$Ni$_3$ + LaNi
7	2	53	45	664↓	L → **(αFe)** → La$_2$Ni$_3$ → LaNi	650	(αFe) + La$_2$Ni$_3$ + LaNi
8	1	50	49	691↓	L → **LaNi** → La$_2$Ni$_3$ → eutectic ((αFe) + La$_2$Ni$_3$ + LaNi)	655	(αFe) + LaNi
9	1	52	47	686↓	L → **LaNi** → La$_2$Ni$_3$ → eutectic ((αFe) + La2Ni$_3$ + LaNi)	653	(αFe) + La$_2$Ni$_3$ + LaNi
10	10	25	65	–	L → **(αFe)** → La$_7$Ni$_3$	532	La$_3$Ni + (αFe) + La$_7$Ni$_3$
11	25	55	20	1321	L → **(γFe,Ni)** → LaNi$_5$ → La$_2$Ni$_7$ → La$_2$Ni$_3$ → LaNi	795	La$_2$Ni$_7$ + (γFe,Ni)
12	5	10	85	–	L → **(βLa)** → La$_3$Ni	–	La$_3$Ni + (αFe) + (βLa)
13	2	21	77	548↓	L → **(αFe)** → (βLa) → La$_3$Ni	525	La$_3$Ni + (αFe) + (βLa)
14	10	10	80	–	L → **(αFe)** → (βLa) → La$_3$Ni	526	La$_3$Ni + (αFe) + (βLa)
15	10	25	65	615↓	L → **(αFe)** → La$_3$Ni	533	La$_3$Ni + (αFe)
16	5	75	20	1337	L → **LaNi$_5$** → La$_5$Ni$_{19}$ → La$_2$Ni$_7$ → La$_7$Ni$_{16}$ → La$_2$Ni$_3$	949	LaNi$_5$ + La$_5$Ni$_{19}$
17	5	60	35	1018	L → **LaNi$_5$** → La$_2$Ni$_7$ → La$_2$Ni$_3$ → LaNi	666	(αFe) + La$_2$Ni$_7$ + La$_2$Ni$_3$
18	5	70	25	1282	L → **LaNi$_5$** → La$_5$Ni$_{19}$ → La$_2$Ni$_7$ → La$_7$Ni$_{16}$ → La$_2$Ni$_3$	667	La$_2$Ni$_7$ + La$_2$Ni$_3$
19	15	65	20	1273	L → **LaNi$_5$** → La$_2$Ni$_7$ → La$_2$Ni$_3$	846	La$_2$Ni$_7$ + LaNi$_5$
20	2	18	80	541	L → **(βLa)** → La$_3$Ni → eutectic ((αFe) + (βLa) + La$_3$Ni)	526	(αFe) + (βLa) + La$_3$Ni
21	2	28	70	–	L → **(αFe)** → La$_7$Ni$_3$	532	(αFe) + La$_3$Ni + La$_7$Ni$_3$
22	2	33	65	558↓	L → **(αFe)** → eutectic (LaNi + La$_7$Ni$_3$)	525	(αFe) + LaNi + La$_7$Ni$_3$
23	10	45	45	–	L → **(γFe,Ni)** → LaNi → eutectic ?	651	LaNi + (αFe)
24	2	68	30	1170	L → **LaNi$_5$** → La$_2$Ni$_7$ → LaNi$_3$ → La$_7$Ni$_{16}$ → La$_2$Ni$_3$	668	La$_7$Ni$_{16}$ + La$_2$Ni$_3$ + LaNi$_3$
25	2	73	25	1279	L → **LaNi$_5$** → La$_2$Ni$_7$ → LaNi$_3$ → La$_7$Ni$_{16}$ → La$_2$Ni$_3$	669	La$_7$Ni$_{16}$ + LaNi$_3$
26	60	25	15	1421	L → **(γFe,Ni)** → La$_2$Ni$_7$ → La$_2$Ni$_3$ → LaNi	667	(αFe) + La$_2$Ni$_3$ + La$_2$Ni$_7$
27	40	25	35	–	L → **(γFe,Ni)** → LaNi → La$_7$Ni$_3$ → eutectic (La$_7$Ni$_3$ + LaNi)	525	(αFe) + LaNi + La$_7$Ni$_3$
28	5	45	50	671↓	L → **(αFe)** → LaNi → La$_7$Ni$_3$ → eutectic (LaNi + La$_7$Ni$_3$)	524	LaNi + (αFe) + La$_7$Ni$_3$
29	5	35	60	616	L → **(αFe)** → LaNi → La$_7$Ni$_3$ → eutectic (LaNi + La$_7$Ni$_3$)	524	LaNi + (αFe) + La$_7$Ni$_3$
30	1	27	72	533↓	L → **La$_7$Ni$_3$** → La$_3$Ni → eutectic ((αFe) + La$_7$Ni$_3$ + La$_3$Ni)	531	(αFe) + La$_3$Ni + La$_7$Ni$_3$
31	2	20	78	538↓	L → **(βLa)** → La$_3$Ni → eutectic ((αFe) + (βLa) + La$_3$Ni)	526	La$_3$Ni + (αFe) + (βLa)
32	10	75	15	1320	L → **LaNi$_5$** → eutectic ((γFe,Ni) + LaNi$_5$)	1251	LaNi$_5$ + (γFe,Ni)
33	10	70	20	1302	L → **LaNi$_5$** → La$_5$Ni$_{19}$ → La$_2$Ni$_7$ → La$_2$Ni$_3$	900	LaNi$_5$ + La$_5$Ni$_{19}$
34	8	40	52	692↓	L → **(αFe)** → LaNi → eutectic (LaNi + La$_7$Ni$_3$)	524	(αFe) + LaNi + La$_7$Ni$_3$
35	20	70	10	1331↓	L → **LaNi$_5$** → eutectic ((γFe,Ni) + LaNi$_5$)	1265	(γFe,Ni) + LaNi$_5$
36	25	40	35	1298	L → **(γFe,Ni)** → LaNi → La$_2$Ni$_3$	653	(αFe) + LaNi + La$_2$Ni$_3$
37	75	10	15	1456	L → **(γFe,Ni)** → eutectic (LaNi + La$_7$Ni$_3$)	524	(αFe) + LaNi + La$_7$Ni$_3$
38	20	55	25	1262	L → **(γFe,Ni)** → LaNi$_5$ → La$_2$Ni$_7$ → La$_2$Ni$_3$ → LaNi	663	(αFe) + La$_2$Ni$_3$ + La$_2$Ni$_7$
39	55	10	35	1425	L → **(γFe,Ni)** → (βLa) → La$_3$Ni	525	La$_3$Ni + (αFe) + (βLa)
40	50	35	15	1411	L → **(γFe,Ni)** → LaNi → La$_2$Ni$_3$	665	(αFe) + La$_2$Ni$_3$ + La$_2$Ni$_7$
41	40	45	15	1374	L → **(γFe,Ni)** → LaNi$_5$ → La$_2$Ni$_7$ → La$_2$Ni$_3$	803	La$_5$Ni$_{19}$ + (γFe,Ni)
42	20	60	20	1272	L → **(γFe,Ni)** → LaNi$_5$ → La$_2$Ni$_7$ → La$_2$Ni$_3$ → LaNi	796	La$_5$Ni$_{19}$ + (γFe,Ni)

[a] Primary phase is shown in bold.
[b] ↓ - DTA data on cooling.

composition of the liquid U_4, which contains no more than 1 at.% Fe. The intersection of the monovariant curves L + La$_2$Ni$_7$ ⇄ LaNi$_3$ (p_6U_5) and L + LaNi$_3$ ⇄ La$_2$Ni$_3$ (U_4U_5) gives the composition of the liquid U_5, which cannot contain more than 1.5 at.% Fe (Fig. 6 *a, c*).

The boundaries of the fields of primary crystallization of phases La$_2$Ni$_3$, LaNi, La$_7$Ni$_3$ and La$_3$Ni were determined mainly from the microstructure of the alloys located along the isoconcentrates 1Fe and 2Fe. A very small amount of the primary (αFe) phase in alloys #7 and #22 indicates that the field of primary crystallization of the LaNi phase do not extend into the ternary system further than up to 2 at.% Fe. The monovariant curve L ⇄ (αFe) + LaNi ($E_1e_5U_7$) of the joint crystallization of the (αFe) and LaNi phases was constructed from the observation of primary (αFe) in alloys #7 and #22 in contrast to primary LaNi in alloys ##1, 8, 9 (Fig. 7 *l*). Moreover, in last three alloys, after the primary crystallization of the LaNi phase, the La$_2$Ni$_3$ phase is formed, and the crystallization ends with the formation of the ternary eutectic (αFe) + La$_2$Ni$_3$ + LaNi (Fig. 7 *l*). The composition of this ternary eutectic according to the EPMA data of the alloys #1 and #9 is 1.8Fe-52.3Ni-45.9La (Table 5).

The observation of a very small amount of the primary crystals of the (αFe)-phase in alloys #21 and 22 with a typical cubic shape of crystals indicates that the field of primary crystallization of the

La$_7$Ni$_3$ phase also does not extend into the ternary system more than up to 2 at.% Fe. The location of the curve L ⇄ (αFe) + La$_7$Ni$_3$ ($U_7e_8E_2$) of the joint crystallization of the (αFe) and La$_7$Ni$_3$ phases is evident from the observation of the primary La$_7$Ni$_3$ in sample #30 in contrast to (αFe) in samples #21 and #22. In the alloy # 30 after primary crystallization of the La$_7$Ni$_3$ phase, the La$_3$Ni phase crystallizes and the solidification finishes with the formation of the ternary eutectic (αFe) + La$_7$Ni$_3$ + La$_3$Ni.

The isotherms in the liquidus surface (Fig. 6 *a*) were constructed based on DTA results (Table 4), and were additionally refined via the constructed vertical sections, so that each alloy was involved in at least two sections.

4.2.3. Solidus projection and invariant equilibria

Fig. 6 *b* shows the solidus surface projection of the La−Ni−Fe system in the whole composition range resulting from this research. The solidus projection was plotted on the basis of a study of as-cast specimens and after the heat treatment at the subsolidus temperatures.

The solidus surface of this system is characterized by the co-existence of (γFe,Ni) and (αFe)-phases with almost all phases from the boundary systems, forming eight three-phase fields

Table 5
Composition of the La−Ni−Fe phases according to EPMA examinations.

#	Alloy composition, at.% nominal			measured			Heat-treatment	EPMA data, at.%			
	Fe	Ni	La	Fe	Ni	La		Phase	Fe	Ni	La
1	1.5	52.5	46.0	1.5	52.4	46.1	as-cast	(αFe)	97.7	1.5	0.8
								La_2Ni_3	0.5 ± 0.1	58.1 ± 0.1	41.4 ± 0.2
								LaNi	0.1 ± 0.1	49.0 ± 0.2	50.9 ± 0.3
								eutectic ((αFe)+La_2Ni_3+LaNi)	1.7	52.2	46.0
									1.9	52.4	45.8
				1.3	52.4	46.3	640°C, 6 h	(αFe)	97.7	1.4	0.9
								La_2Ni_3	0.7 ± 0.1	58.1 ± 0.1	41.2 ± 0.1
								LaNi	0.1 ± 0.1	48.7 ± 0.1	51.2 ± 0.1
2	3	57	40	2.4	56.8	40.8	as-cast	La_2Ni_7	10.4 ± 0.5	65.9 ± 0.7	23.7 ± 0.1
								La_2Ni_3	0.9 ± 0.1	57.8 ± 0.2	41.3 ± 0.1
								LaNi	0.0 ± 0.0	49.1 ± 0.5	50.9 ± 0.5
3	30	55	15	30.9	53.9	15.2	as-cast	(γFe,Ni)	59.2 ± 0.2	40.1 ± 0.2	0.7 ± 0.1
								$LaNi_5$	19.7 ± 0.8	63.0 ± 0.9	17.3 ± 0.1
								La_2Ni_7	14.0 ± 0.3	63.1 ± 0.3	22.9 ± 0.1
								La_2Ni_3	2.0 ± 0.3	56.8 ± 0.3	41.2 ± 0.1
				30.0	53.7	16.3	815 °C, 6 h	(γFe,Ni)	86.5	12.4	0.9
								$LaNi_5$	21.9 ± 0.4	60.3 ± 0.4	17.8 ± 0.1
								La_5Ni_{19}	16.1 ± 0.2	62.1 ± 0.1	21.8 ± 0.1
4	10	60	30	9.8	58.7	31.5	as-cast	$LaNi_5$	20.9 ± 0.3	61.3 ± 0.3	17.8 ± 0.1
								La_2Ni_7	13.9 ± 0.9	62.7 ± 0.9	23.4 ± 0.1
								La_2Ni_3	1.1 ± 0.2	57.7 ± 0.2	41.1 ± 0.2
								LaNi	0.1 ± 0.2	49.8 ± 0.3	50.1 ± 0.4
				10.0	58.8	31.3	660 °C, 6 h	(αFe)	96.1 ± 0.1	3.0 ± 0.1	0.9 ± 0.1
								La_2Ni_7	12.9 ± 0.1	63.8 ± 0.1	23.3 ± 0.1
								La_2Ni_3	0.8 ± 0.3	58.0 ± 0.2	41.2 ± 0.2
5	10	55	35	9.5	55.5	35.0	as-cast	(γFe,Ni)	82.8 ± 0.8	16.4 ± 0.3	0.8 ± 0.7
								$LaNi_5$	19.9 ± 0.1	62.2 ± 0.3	17.9 ± 0.2
								La_2Ni_7	13.5 ± 0.2	63.3 ± 0.1	23.1 ± 0.1
								La_2Ni_3	1.2 ± 0.2	58.2 ± 0.3	40.6 ± 0.3
								LaNi	0.4 ± 0.3	49.9 ± 0.7	49.7 ± 0.6
6	5	55	40	2.7	54.9	42.4	as-cast	La_2Ni_7	14.0 ± 0.6	62.4 ± 0.6	23.6 ± 0.2
								La_2Ni_3	0.9 ± 0.1	58.0 ± 0.2	41.1 ± 0.2
								LaNi	0.1 ± 0.1	49.4 ± 0.1	50.6 ± 0.1
7	2	53	45	1.9	52.1	46.0	as-cast	(αFe)	97.3	2.3	0.4
								La_2Ni_3	1.1 ± 0.3	57.6 ± 0.4	41.3 ± 0.1
								LaNi	0.0 ± 0.0	49.1 ± 0.1	50.9 ± 0.1
8	1	50	49	0.5	49.1	50.4	as-cast	La_2Ni_3	0.9 ± 0.2	57.5 ± 0.2	41.6 ± 0.2
								LaNi	0.0 ± 0.0	48.8 ± 0.2	51.2 ± 0.2
9	1	52	47	0.9	52.1	47.0	as-cast	La_2Ni_3	0.8 ± 0.1	57.6 ± 0.2	41.6 ± 0.2
								LaNi	0.2 ± 0.1	48.5 ± 0.2	51.3 ± 0.2
								eutectic ((αFe)+La_2Ni_3+LaNi)	1.8	52.3	45.9
									1.7	52.4	45.9
11	25	55	20	26.0	53.9	20.1	as-cast	(γFe,Ni)	64.2 ± 0.2	34.9 ± 0.2	0.9 ± 0.1
								$LaNi_5$	20.2 ± 0.7	62.3 ± 0.6	17.5 ± 0.1
								La_2Ni_7	13.4 ± 0.5	63.3 ± 0.5	23.4 ± 0.3
								La_2Ni_3	1.9 ± 0.2	57.5 ± 0.2	40.6 ± 0.1
								LaNi	0.9 ± 0.2	48.9 ± 0.2	50.2 ± 0.2
				25.0	54.8	20.2	780 °C, 15 h	(γFe,Ni)	90.3 ± 0.4	9.1 ± 0.5	0.7 ± 0.1
								La_2Ni_7	14.0 ± 0.2	62.7 ± 0.2	23.3 ± 0.1
12	5	10	85	4.7	10.2	85.1	as-cast	(βLa)	0.1 ± 0.1	0.0 ± 0.0	99.9 ± 0.1
								La_3Ni	0.0 ± 0.0	23.4 ± 0.1	76.6 ± 0.1
				−	−	−	510 °C, 6 h	(βLa)	0.0 ± 0.0	0.0 ± 0.0	100.0 ± 0.0
								La_3Ni	0.1 ± 0.1	23.8 ± 0.2	76.1 ± 0.2
								(αFe)	99.0 ± 0.2	0.1 ± 0.1	0.9 ± 0.2
13	2	21	77	2.0	20.4	77.6	as-cast	(βLa)	0.0 ± 0.0	0.8 ± 0.3	99.2 ± 0.3
								(αFe)	98.9	0.2	0.9
								La_3Ni	0.6 ± 0.3	23.2 ± 0.2	76.2 ± 0.2
14	10	10	80	8.9	10.0	81.1	as-cast	(αFe)	99.1 ± 0.1	0.0 ± 0.0	0.9 ± 0.1
								(βLa)	0.0 ± 0.0	0.0 ± 0.0	100.0 ± 0.0
								La_3Ni	0.0 ± 0.0	23.4 ± 0.3	76.6 ± 0.3
15	10	25	65	10.7	20.8	68.5	as-cast	(αFe)	98.9 ± 0.6	0.2 ± 0.2	0.9 ± 0.3
								La_3Ni	0.5 ± 0.1	23.2 ± 0.1	76.3 ± 0.3
16	5	75	20	4.8	74.0	21.2	as-cast	$LaNi_5$	6.5 ± 0.2	75.9 ± 0.1	17.7 ± 0.1
								La_2Ni_7	3.7	72.4	23.9
								La_7Ni_{16}	0.5 ± 0.1	66.8 ± 0.1	32.7 ± 0.1
								La_2Ni_3	0.1 ± 0.1	58.9 ± 0.2	41.0 ± 0.3
17	10	60	30	9.8	58.7	31.5	as-cast	$LaNi_5$	20.9 ± 0.3	61.3 ± 0.3	17.8 ± 0.2
								La_2Ni_7	13.9 ± 0.9	62.7 ± 0.9	23.4 ± 0.2
								La_2Ni_3	1.1 ± 0.2	57.7 ± 0.2	41.1 ± 0.2
								LaNi	0.1 ± 0.2	49.8 ± 0.3	50.1 ± 0.4
18	5	70	25	5.0	68.6	26.3	as-cast	$LaNi_5$	7.0 ± 0.1	75.4 ± 0.1	17.7 ± 0.1
								La_5Ni_{19}	6.0	72.2	21.8
								La_2Ni_7	5.8 ± 0.2	71.0 ± 0.2	23.2 ± 0.1

Table 5 (*continued*)

								La_7Ni_{16}	0.1 ± 0.0	67.2 ± 0.2	32.7 ± 0.2
								La_2Ni_3	0.6 ± 0.4	58.9 ± 0.4	40.8 ± 0.3
19	15	65	20	15.1	63.6	21.3	as-cast	$LaNi_5$	17.9 ± 0.1	64.7 ± 0.1	17.4 ± 0.1
								La_2Ni_7	12.8 ± 0.6	63.9 ± 0.8	23.3 ± 0.3
								La_2Ni_3	1.8 ± 0.2	57.8 ± 0.4	40.4 ± 0.3
20	2	18	80	2.0	18.6	79.4	as-cast	(βLa)	0.0 ± 0.0	0.0 ± 0.0	100.0 ± 0.0
								La_3Ni	0.5 ± 0.3	23.3 ± 0.3	76.2 ± 0.4
								eutectic $((\alpha Fe)+(\beta La)+La_3Ni)$	1.4	21.3	77.3
									1.5	21.1	77.4
21	2	28	70	1.5	27.4	71.1	as-cast	(αFe)	98.8	0.6	0.6
								La_7Ni_3	0.3 ± 0.4	28.5 ± 0.4	71.2 ± 0.4
22	2	33	65	1.7	32.5	65.8	as-cast	(αFe)	99.0 ± 0.3	0.2 ± 0.3	0.8 ± 0.1
								eutectic $(LaNi + La_7Ni_3)$	0.1	33.9	66.0
									0.1	33.4	66.5
23	10	45	45	10.5	44.0	45.5	as-cast	$(\gamma Fe,Ni)$	92.2	6.7	0.9
								$LaNi$	0.3 ± 0.2	49.0 ± 0.1	50.7 ± 0.2
24	2	68	30	2.0	66.5	31.5	as-cast	$LaNi_5$	5.4 ± 0.2	76.8 ± 0.3	17.8 ± 0.2
								La_2Ni_7	3.3 ± 0.2	73.3 ± 0.4	23.4 ± 0.2
								$LaNi_3$	2.3 ± 0.2	71.3 ± 0.3	26.4 ± 0.2
								La_7Ni_{16}	0.2 ± 0.2	67.3 ± 0.3	32.5 ± 0.1
								La_2Ni_3	0.1 ± 0.0	58.7 ± 0.1	41.2 ± 0.1
				1.8	66.6	31.6	660 °C, 8 h	$LaNi_3$	2.7 ± 0.2	70.9 ± 0.2	26.4 ± 0.2
								La_7Ni_{16}	0.5 ± 0.5	67.0 ± 0.5	32.5 ± 0.1
								La_2Ni_3	0.1 ± 0.0	58.6 ± 0.2	41.3 ± 0.2
25	2	73	25	1.9	71.3	26.8	as-cast	$LaNi_5$	3.2 ± 0.1	78.9 ± 0.2	17.9 ± 0.1
								La_5Ni_{19}	2.5	75.3	22.2
								La_2Ni_7	2.4 ± 0.1	74.1 ± 0.1	23.5 ± 0.1
								$LaNi_3$	1.8 ± 0.1	72.0 ± 0.2	26.2 ± 0.1
								La_7Ni_{16}	0.1 ± 0.1	67.2 ± 0.1	32.7 ± 0.1
								La_2Ni_3	0.1	58.5	41.4
				1.9	71.2	26.9	660 °C, 15 h	$LaNi_3$	2.1 ± 0.2	71.3 ± 0.2	26.6 ± 0.1
								La_7Ni_{16}	0.2 ± 0.1	67.0 ± 0.1	32.8 ± 0.1
26	60	25	15	59.7	25.4	14.9	as-cast	$(\gamma Fe,Ni)$	88.6 ± 0.1	10.7 ± 0.2	0.7 ± 0.1
27	40	25	35	37.9	25.3	36.8	as-cast	$(\gamma Fe,Ni)$	95.4 ± 0.1	3.9 ± 0.1	0.7 ± 0.1
								$LaNi$	0.4 ± 0.5	48.7 ± 0.6	51.0 ± 0.2
								La_7Ni_3	0.0 ± 0.0	29.5 ± 0.3	70.5 ± 0.3
28	5	45	50	5.1	44.0	50.9	as-cast	(αFe)	96.6	2.5	0.9
								$LaNi$	0.0 ± 0.0	48.9 ± 0.1	51.1 ± 0.1
								La_7Ni_3	0.0 ± 0.0	29.7 ± 0.1	70.4 ± 0.1
29	5	35	60	4.6	35.7	59.7	as-cast	(αFe)	97.5	1.6	0.9
								$LaNi$	0.0 ± 0.0	48.4 ± 0.1	51.6 ± 0.1
								La_7Ni_3	0.0 ± 0.0	28.9 ± 0.3	71.1 ± 0.3
				4.6	35.7	59.7	510 °C, 6 h	(αFe)	97.6 ± 0.1	1.5 ± 0.1	0.9 ± 0.1
								$LaNi$	0.2 ± 0.1	48.4 ± 0.1	51.4 ± 0.2
								La_7Ni_3	0.1 ± 0.1	28.9 ± 0.2	71.1 ± 0.3
30	1	27	72	1.1	26.8	72.1	520 °C, 6 h	(αFe)	97.5	1.6	0.8
								La_7Ni_3	0.2	28.3	71.5
								La_3Ni	0.1 ± 0.1	24.1 ± 0.2	75.8 ± 0.2
31	2	20	78	1.9	20.1	78.0	as-cast	(βLa)	0.0 ± 0.0	0.0 ± 0.0	100.0 ± 0.0
								La_3Ni	0.2 ± 0.2	24.0 ± 0.3	75.8 ± 0.4
								eutectic $((\alpha Fe)+(\beta La)+La_3Ni)$	1.4	21.3	77.3
									1.3	21.3	77.4
32	10	75	15	10.0	74.0	16.0	as-cast	$LaNi_5$	6.9 ± 0.4	75.8 ± 0.3	17.3 ± 0.1
								eutectic $((\gamma Fe,Ni)+LaNi_5)$	19.9	68.8	11.3
									19.6	69.4	11.0
									19.5	69.5	11.2
									20.9	68.8	10.3
33	10	70	20	9.9	69.2	20.9	as-cast	$LaNi_5$	12.1 ± 0.1	70.6 ± 0.1	17.4 ± 0.2
								La_5Ni_{19}	9.7	68.5	21.8
								La_2Ni_7	8.8 ± 0.4	68.5 ± 0.4	22.7 ± 0.2
				10.2	68.6	21.2	850 °C, 2 h	$LaNi_5$	12.5 ± 0.3	69.7 ± 0.3	17.8 ± 0.1
								La_5Ni_{19}	9.7 ± 0.4	68.7 ± 0.3	21.6 ± 0.2
34	8	40	52	7.5	39.8	52.7	as-cast	(αFe)	97.6	1.5	0.9
								La_7Ni_3	0.0	30.2	69.8
								$LaNi$	0.9 ± 0.8	48.2 ± 0.1	50.9 ± 0.8
35	20	70	10	20.5	69.5	10.0	as-cast	$LaNi_5$	10.1 ± 0.1	72.9 ± 0.1	17.0 ± 0.1
								$(\gamma Fe,Ni)$	34.9 ± 0.4	64.4 ± 0.5	0.7 ± 0.2
								eutectic $((\gamma Fe,Ni)+LaNi_5)$	20.62	69.65	9.74
									20.68	69.43	9.89
									20.99	69	10
									20.05	69.98	9.97
36	25	40	35	23.9	39.5	36.6	as-cast	$(\gamma Fe,Ni)$	90.6 ± 0.2	8.3 ± 0.2	0.9 ± 0.1
								La_2Ni_3	1.3 ± 0.5	57.2 ± 0.4	41.5 ± 0.2
								$LaNi$	0.1 ± 0.1	48,5 ± 0.2	51.4 ± 0.2
42	20	60	20	18.9	60.1	21.0	790 °C, 8 h	$(\gamma Fe,Ni)$	89.2	10.1	0.7
								La_5Ni_{19}	15.9 ± 0.1	62.6 ± 0.1	215 ± 0.1
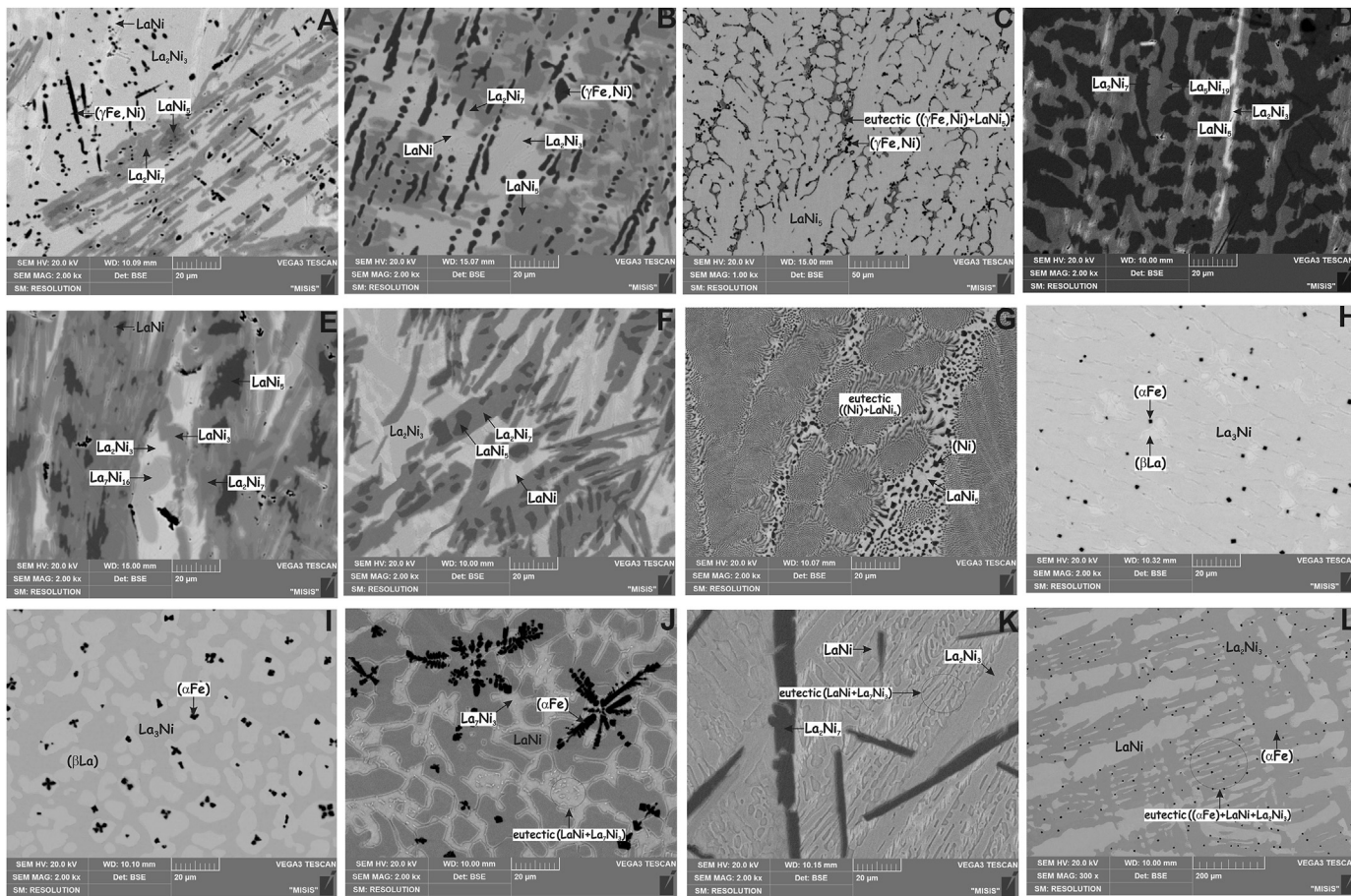
Fig. 7. Microstructure of as-cast alloys of the La−Ni−Fe system:
a − 10Fe−55Ni−35La (#5), × 2000, (γFe,Ni) + LaNi$_5$ + La$_2$Ni$_7$ + La$_2$Ni$_3$ + LaNi;
b − 25Fe−55Ni−20La (#11), × 2000, (γFe,Ni) + LaNi$_5$ + La$_2$Ni$_7$ + La$_2$Ni$_3$ + LaNi;
c − 10Fe−75Ni−15La (#32) × 1000, LaNi$_5$ + eutectic ((γFe,Ni) + LaNi$_5$));
d − 10Fe−70Ni−20La (#33), × 2000, LaNi$_5$ + La$_5$Ni$_{19}$ + La$_2$Ni$_7$ + La$_2$Ni$_3$;
e − 2Fe−73Ni−25La (#25) × 2000, LaNi$_5$ + La$_2$Ni$_7$ + LaNi$_3$ + La$_7$Ni$_{16}$ + La$_2$Ni$_3$;
f − 10Fe−60Ni−30La (#4) × 2000, LaNi$_5$ + La$_2$Ni$_7$ + La$_2$Ni$_3$ + LaNi;
g − 20Fe−70Ni−10La (#35) × 2000, eutectic ((γFe,Ni) + LaNi$_5$));
h − 2Fe−21Ni−77La (#13), × 2000, (αFe) + La$_3$Ni + (βLa);
i − 10Fe−10Ni−80La (#14), × 2000, (γFe,Ni) + (βLa) + La$_3$Ni;
j − 8Fe−40Ni−52La (#34) × 2000, (αFe) + LaNi + eutectic (LaNi + La$_7$Ni$_3$);
k − 5Fe−55Ni−40La (#6), × 2000, La$_2$Ni$_7$ + La$_2$Ni$_3$ + LaNi + eutectic (LaNi + La$_2$Ni$_3$);
l − 1Fe−52Ni−47La (#9), × 300, LaNi + La$_2$Ni$_3$ + eutectic ((αFe) + LaNi + La$_2$Ni$_3$).

(γFe,Ni) + LaNi$_5$ + La$_5$Ni$_{19}$, (γFe,Ni) + La$_5$Ni$_{19}$ + La$_2$Ni$_7$, (γFe,Ni) + (αFe) + La$_2$Ni$_7$, (αFe) + La$_2$Ni$_7$ + La$_2$Ni$_3$, (αFe) + LaNi + La$_2$Ni$_3$, (αFe) + LaNi + La$_7$Ni$_3$, (αFe) + La$_3$Ni + La$_7$Ni$_3$, (αFe) + La$_3$Ni + (βLa) and appropriate two-phase regions. Two narrower three-phase regions without the participation of the (γFe,Ni) and (αFe)-phases are present in the La−Ni−Fe system: La$_2$Ni$_7$ + LaNi$_3$ + La$_2$Ni$_3$ and La$_2$Ni$_3$ + LaNi$_3$ + La$_7$Ni$_{16}$. The corners of these triangles were plotted using the microprobe results for individual phases (Table 5). The solidus temperatures of three-phase regions, as measured by DTA (Table 4), are shown in the solidus projection (Fig. 6 b).

Fig. 8 a represents the micrograph of sample #3 annealed at subsolidus temperature (815 °C, 6 h). Evidently, this alloy is in a three-phase equilibrium (γFe,Ni) + LaNi$_5$ + La$_5$Ni$_{19}$. The boundaries of this three-phase region were established based on SEM and EPMA data. The heating curve of this alloy shows an invariant effect at 824 °C (Table 4). In samples ##4, 5, 11, 38, 40−42 the thermal effect at 824 °C was also observed, corresponding to four-phase invariant equilibrium L + (γFe,Ni) + LaNi$_5$ + La$_5$Ni$_{19}$ and resulting

in formation of narrow (γFe,Ni) + LaNi$_5$ + La$_5$Ni$_{19}$ solidus region. Consequently, this three-phase region forms via transition type reaction L$_{U1}$ + LaNi$_5$ ⇄ (γFe,Ni) + La$_5$Ni$_{19}$ at 824 °C.

Existence of (γFe,Ni) + La$_2$Ni$_7$ (alloys #41 and #42) and (γFe,Ni) + La$_5$Ni$_{19}$ (alloy #11) two-phase equilibria suggest that there should be a three-phase (γFe,Ni) + La$_2$Ni$_7$ + La$_5$Ni$_{19}$ equilibrium. This three-phase region is narrow, and there were no alloys within it, so exact location was not established. However, it cannot differ significantly from that shown in Fig. 6 b due to the proximity of neighboring three-phase areas. The heating DTA curves of the alloys ##4, 5, 11, 38, 40−42 show an invariant effect at 795 °C, which can be ascribed to four-phase invariant equilibrium L + (γFe,Ni) + La$_2$Ni$_7$ + La$_5$Ni$_{19}$, resulting in formation of narrow (γFe,Ni) + La$_2$Ni$_7$ + La$_5$Ni$_{19}$ solidus region. This three-phase region forms via transition type reaction L$_{U2}$ + La$_5$Ni$_{19}$ ⇄ (γFe,Ni) + La$_2$Ni$_7$ at 795 °C.

The three-phase microstructure of annealed at subsolidus temperature (660 °C during 6 h) sample #4 allows to locate this sample within the (αFe) + La$_2$Ni$_7$ + La$_2$Ni$_3$ triangle. Three phases
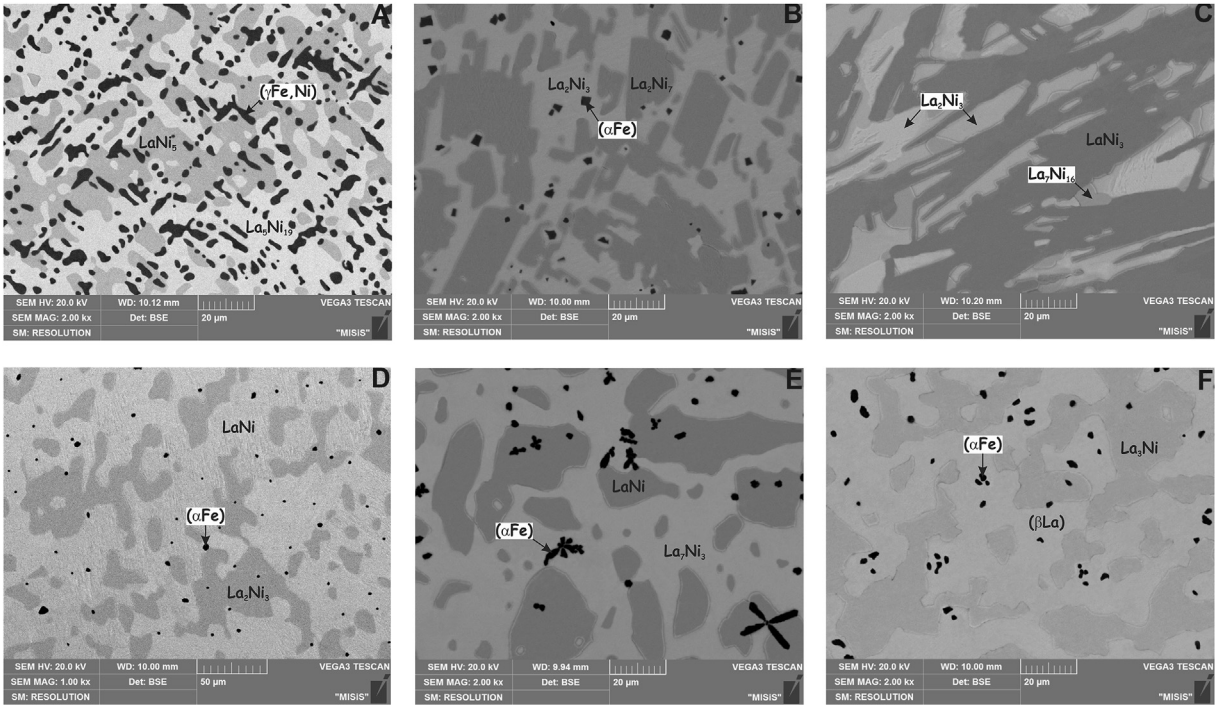
Fig. 8. Microstructure of annealed at subsolidus temperatures alloys of the La−Ni−Fe system:
a − 30Fe−55Ni−15La (#3), 815 °C, × 2000, (γFe,Ni) + LaNi$_5$ + La$_5$Ni$_{19}$;
b − 10Fe−60Ni−30La (#4), 660 °C, × 2000, (αFe) + La$_2$Ni$_7$ + La$_2$Ni$_3$;
c − 2Fe−68Ni−30La (#24), 660 °C, × 2000, La$_7$Ni$_{16}$ + La$_2$Ni$_3$ + LaNi$_3$;
d − 1.5Fe-52.5Ni-46.0La (#1), 640 °C, × 1000, (αFe) + La$_2$Ni$_7$ + La$_2$Ni$_3$ + LaNi;
e − 5Fe−35Ni−60La (#29), 510 °C × 2000, (αFe) + LaNi + La$_7$Ni$_3$;
f − 5Fe−10Ni−85La (#12), 510 °C, × 2000, (βLa) + La$_3$Ni + (αFe).
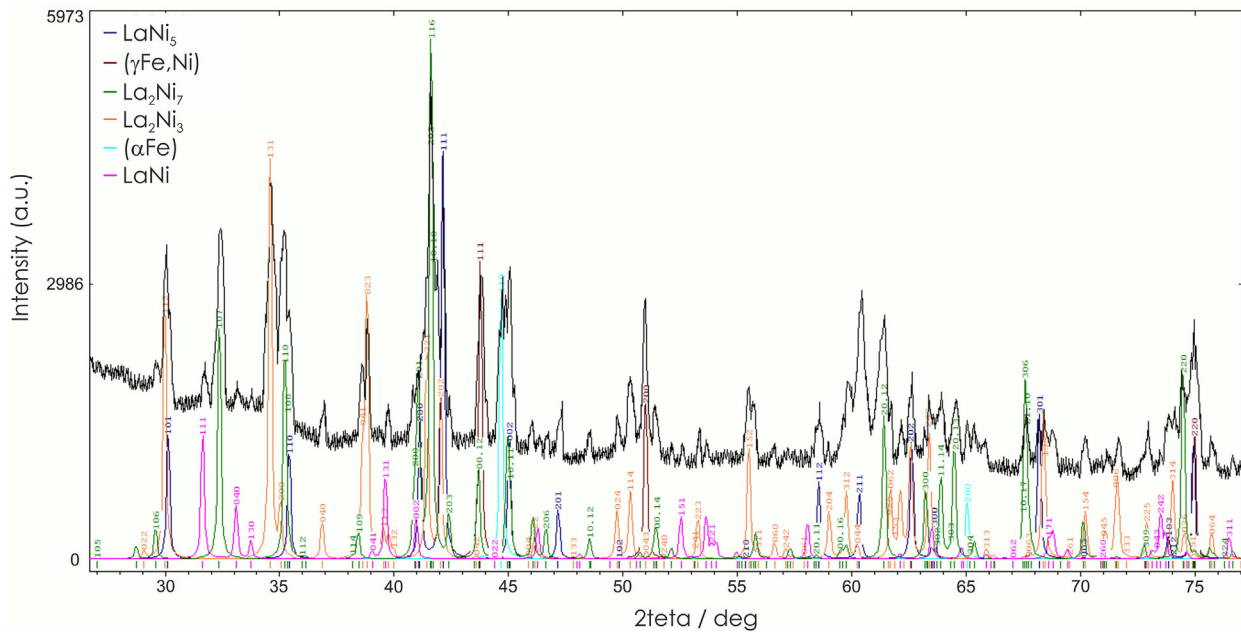
Fig. 9. X-ray diffraction pattern of the as-cast alloy 25Fe−55Ni−20La (#11).

can be well distinguished in microstructure of this alloy (Fig. 8 b). The composition of the solid phases in this equilibrium was measured by microprobe method (Table 5). The heating curve of this alloy, as well as alloys ##5, 17, 26, 38, 40, shows an invariant effect at 665 °C (Table 4). Therefore, this three-phase region also is formed via a U-type reaction $L_{U6} + La_2Ni_7 \rightleftarrows (\alpha Fe) + La_2Ni_3$ at 665 °C.

In view of existence of the isothermal planes $(\gamma Fe, Ni) + La_2Ni_7 + La_5Ni_{19}$ and $(\alpha Fe) + La_2Ni_7 + La_2Ni_3$ (see above), the very narrow isothermal plane $(\gamma Fe, Ni) + (\alpha Fe) + La_2Ni_7$ should also exist. Even though there is no experimental evidence concerning the exact position of this region, it could not differ substantially from that shown in Fig. 6 b. The position of the vertices of the respective tie-line triangle was determined from the mutual arrangement of the regions of phase homogeneity. DTA curves of the samples ##5, 11, 26, 38, 40–42 contained the thermal effect at about 720 °C, which was ascribed to the solidus temperature of this region. This three-phase region also is formed via transition type reaction $L_{U3} + (\gamma Fe, Ni) \rightleftarrows (\alpha Fe) + La_2Ni_7$ at 720 °C.

Two very narrow three-phase regions $La_7Ni_{16} + La_2Ni_3 + LaNi_3$ and $La_2Ni_7 + LaNi_3 + La_2Ni_3$ with the participation of the $LaNi_3$ phase are present on the solidus surface of the La−Ni−Fe system. The microphotograph of the sample #24 annealed at the subsolidus temperature (660 °C during 8 h) is shown in Fig. 8 c. This sample is placed in the tie-triangle $La_7Ni_{16} + La_2Ni_3 + LaNi_3$ and its microstructure clearly shows these three phases. The composition of the solid phases in this equilibrium was measured by microprobe method (Table 5). The heating curve of this alloy shows an invariant effect at 668 °C (Table 4). There were no alloys within the three-phase region $La_2Ni_7 + LaNi_3 + La_2Ni_3$, so exact location of the La_2Ni_7 corner was not established. However, it cannot differ significantly from that shown in Fig. 6 b because the alloy #18 is two-phase $La_2Ni_7 + La_2Ni_3$. The solidus temperature of this isothermal plane was estimated as 667 °C. Both three-phase regions $La_7Ni_{16} + La_2Ni_3 + LaNi_3$ and $La_2Ni_7 + LaNi_3 + La_2Ni_3$ are formed by transition type reactions $L_{U4} + La_7Ni_{16} \rightleftarrows LaNi_3 + La_2Ni_3$ and $L_{U5} + LaNi_3 \rightleftarrows La_2Ni_7 + La_2Ni_3$ at 668 and 667 °C, respectively.

The alloy #1 annealed at subsolidus temperature (640 °C during 6 h) is located in three-phase region $(\alpha Fe) + La_2Ni_3 + LaNi$ (Tables 4 and 5, Fig. 8 d). According to the DTA data of this alloy, as well as alloys ##6, 7, 9, 36, the temperature of the corresponding isothermal plane is 652 °C (Table 4). This three-phase region is formed due to the occurrence of four-phase invariant equilibrium of the eutectic type $L \rightleftarrows (\alpha Fe) + La_2Ni_3 + LaNi$ at 652 °C. Location of the invariant liquid point within this three-phase field in the solidus projection evidence that equilibrium is of eutectic type. The eutectic type of this equilibrium is also confirmed by observation of the ternary eutectic $((\alpha Fe) + La_2Ni_3 + LaNi)$ on microstructure of the alloys ##1, 8, 9 (Fig. 7 l). Composition of this eutectic was established by the microprobe method for these alloys. Moreover, the solidus temperature of the three-phase field $(\alpha Fe) + La_2Ni_3 + LaNi$ is lower than the temperature of the eutectic $L \rightleftarrows La_2Ni_3 + LaNi$ (DTA analysis of the binary alloy 45La−55Ni (Fig. 1 e, Table 2) indicates the temperature of the eutectic reaction $L \rightleftarrows La_2Ni_3 + LaNi$ to be 658 °C).

The existence of the three-phase region $(\alpha Fe) + LaNi + La_7Ni_3$ and its location were established based on the results of SEM and EPMA of alloy #29 which was annealed at 510 °C during 6 h (Tables 4 and 5, Fig. 8 e). The microstructure of this sample definitely shows three phases: dark, grey and light-grey (Fig. 8 e). These correspond to (αFe), $LaNi$ and La_7Ni_3, respectively. The heating curves of this alloy, as well as alloys ##22, 27, 28, 34, 37, show that the temperature of the respective isothermal plane $(\alpha Fe) + LaNi + La_7Ni_3$ is 524 °C (Table 4). This three-phase region of the solidus surface results from a four-phase invariant transition

type reaction $L_{U7} + (\alpha Fe) \rightleftarrows LaNi + La_7Ni_3$ at 524 °C, rather than a eutectic type. The arguments for this conclusion are as follows: (1) the solidus temperature of the field $(\alpha Fe) + LaNi + La_7Ni_3$ is higher than the temperature of the eutectic $L \rightleftarrows LaNi + La_7Ni_3$ (DTA analysis of the almost eutectic binary alloy 65La−35Ni indicates the temperature of the eutectic reaction $L \rightleftarrows LaNi + La_7Ni_3$ to be 523 °C (Fig. 1 f, Table 2)); (2) in alloys ##22, 27−29, 34, 37 the binary eutectic $(LaNi + La_7Ni_3)$ was observed. This could not have been observed in these alloys if the invariant equilibrium was of the eutectic type $L \rightleftarrows (\alpha Fe) + LaNi + La_7Ni_3$.

According to the SEM and EPMA results the alloy #30, annealed at the subsolidus temperature (520 °C/6 h), is located in the three-phase $(\alpha Fe) + La_7Ni_3 + La_3Ni$ region. The DTA curves of samples ##10, 21, 30 shows the solidus temperature 532 °C (Table 4), indicating their location within the same three-phase region $(\alpha Fe) + La_7Ni_3 + La_3Ni$. This three-phase region also forms via eutectic type reaction $L_{E2} \rightleftarrows (\alpha Fe) + La_7Ni_3 + La_3Ni$ at 532 °C. The eutectic type of this equilibrium is also confirmed by observation of the ternary eutectic $((\alpha Fe) + La_3Ni + La_7Ni_3)$ on microstructure of the alloys #21 and #30. Moreover, the solidus temperature of the three-phase field $(\alpha Fe) + La_3Ni + La_7Ni_3$ is lower than the temperature of the binary eutectic $L \rightleftarrows La_3Ni + La_7Ni_3$ (DTA analysis of the binary eutectic alloy 74.5La-25.5Ni (Fig. 1 g, Table 2) indicates the temperature of the eutectic reaction $L \rightleftarrows La_3Ni + La_7Ni_3$ to be 534 °C).

The boundaries of three-phase region $(\alpha Fe) + La_3Ni + (\beta La)$ were established based on SEM and EPMA data for the three-phase alloy #12 annealed at the subsolidus temperature (510 °C/6 h) (Tables 4 and 5, Fig. 8 f). In microstructure of this alloy, which is shown in Fig. 8 f, three phases $(\alpha Fe) + La_3Ni + (\beta La)$ are well distinguished. The temperature of this isothermal plane was measured as 524 °C (Table 4). This three-phase region also forms via eutectic type reaction $L_{E3} \rightleftarrows (\alpha Fe) + La_3Ni + (\beta La)$ at 524 °C. The eutectic type of this equilibrium is confirmed by observation of the ternary eutectic $((\alpha Fe) + La_3Ni + (\beta La))$ on microstructure of the alloys #20 and #31. Composition of this eutectic was established by the microprobe method for this alloy. Moreover, the solidus temperature of the three-phase field $(\alpha Fe) + La_3Ni + (\beta La)$ is lower than the temperature of the eutectic $L \rightleftarrows La_3Ni + (\beta La)$ (DTA analysis of the binary eutectic alloy 77La−23Ni indicates the temperature of the eutectic reaction $L \rightleftarrows La_3Ni + (\beta La)$ to be 531 °C (Fig. 1 h, Table 2)).

The superposition of the liquidus and solidus surfaces, shown as the melting diagram, is given in Fig. 6 c. The three-phase regions of the solidus surface are the result of three eutectic type and remaining U-type four-phase invariant equilibria $L_{U1} + LaNi_5 \rightleftarrows (\gamma Fe, Ni) + La_5Ni_{19}$, $L_{U2} + La_5Ni_{19} \rightleftarrows (\gamma Fe, Ni) + La_2Ni_7$, $L_{U3} + (\gamma Fe, Ni)$

Table 6
Invariant equilibria in the La−Ni−Fe system.

Type	Invariant equilibria	Temperature, °C	Composition of liquid, at.%		
			Fe	Ni	La
U_1	$L_{U1} + LaNi_5 \rightleftarrows (\gamma Fe, Ni) + La_5Ni_{19}$	824	6	56	38
U_2	$L_{U2} + La_5Ni_{19} \rightleftarrows (\gamma Fe, Ni) + La_2Ni_7$	795	5.5	55.5	39
U_3	$L_{U3} + (\gamma Fe, Ni) \rightleftarrows (\alpha Fe) + La_2Ni_7$	720	4.5	55	40.5
U_4	$L_{U4} + La_7Ni_{16} \rightleftarrows La_2Ni_3 + LaNi_3$	668	1	56.5	42.5
U_5	$L_{U5} + LaNi_3 \rightleftarrows La_2Ni_7 + La_2Ni_3$	667	1.5	56	42.5
U_6	$L_{U6} + La_2Ni_7 \rightleftarrows (\alpha Fe) + La_2Ni_3$	665	2.5	54	43.5
U_7	$L_{U7} + (\alpha Fe) \rightleftarrows LaNi + La_7Ni_3$	524	0.5	34	65.5
E_1	$L_{E1} \rightleftarrows (\alpha Fe) + La_2Ni_3 + LaNi$	652	1.8	52.3	45.9
E_2	$L_{E2} \rightleftarrows (\alpha Fe) + La_3Ni + La_7Ni_3$	532	1	25	74
E_3	$L_{E3} \rightleftarrows (\beta La) + (\alpha Fe) + La_3Ni$	525	1.4	21.3	77.3
e_1	$L_{e1} \rightleftarrows (\gamma Fe, Ni) + LaNi_5$	1302	20.5	69.5	10.0
e_5	$L_{e5} \rightleftarrows (\alpha Fe) + LaNi$	655	1	49	50
e_7	$L_{e7} \rightleftarrows (\alpha Fe) + La_3Ni$	533	1	26	75
e_8	$L_{e8} \rightleftarrows (\alpha Fe) + La_7Ni_3$	>532	1	29	70

Fe-Ni	Fe-La	Fe-Ni-La	La-Ni

Fe-Ni

1514 | p_1
$L+(\delta Fe)\leftrightarrow(\gamma Fe,Ni)$

Fe-La

1383 | c_1
$(\delta Fe)\leftrightarrow(\gamma Fe)+L$

918 | p_4
$L+(\gamma Fe)\leftrightarrow(\alpha Fe)$

846 | c_2
$(\gamma La)\leftrightarrow(\beta La)+L$

788 | e_3
$L\leftrightarrow(\alpha Fe)+(\beta La)$

Fe-Ni-La

1302 | e_1 (max)
$L\leftrightarrow(\gamma Fe,Ni)+LaNi_5$

824 | $L+LaNi_5\leftrightarrow(\gamma Fe,Ni)+La_5Ni_{19}$ | U_1
$(\gamma Fe,Ni)+La_5Ni_{19}+LaNi_5$

795 | $L+La_5Ni_{19}\leftrightarrow(\gamma Fe,Ni)+La_2Ni_7$ | U_2
$(\gamma Fe,Ni)+La_5Ni_{19}+La_2Ni_7$

720 | $L+(\gamma Fe,Ni)\leftrightarrow(\alpha Fe)+La_2Ni_7$ | U_3
$(\gamma Fe,Ni)+(\alpha Fe)+La_2Ni_7$

668 | $L+La_7Ni_{16}\leftrightarrow LaNi_3+La_2Ni_3$ | U_4
$LaNi_3+La_7Ni_{16}+La_2Ni_3$

667 | $L+LaNi_3\leftrightarrow La_2Ni_7+La_2Ni_3$ | U_5
$LaNi_3+La_2Ni_7+La_2Ni_3$

665 | $L+La_2Ni_7\leftrightarrow(\alpha Fe)+La_2Ni_3$ | U_6
$La_2Ni_7+(\alpha Fe)+La_2Ni_3$

655 | e_5 (max)
$L\leftrightarrow(\alpha Fe)+LaNi$

652 | $L\leftrightarrow(\alpha Fe)+La_2Ni_3+LaNi$ | E_1
$(\alpha Fe)+La_2Ni_3+LaNi$

533 | e_7 (max)
$L\leftrightarrow(\alpha Fe)+La_3Ni$

>532 | e_8 (max)
$L\leftrightarrow(\alpha Fe)+La_7Ni_3$

532 | $L\leftrightarrow(\alpha Fe)+La_3Ni+La_7Ni_3$ | E_2
$(\alpha Fe)+La_3Ni+La_7Ni_3$

525 | $L\leftrightarrow(\beta La)+(\alpha Fe)+La_3Ni$ | E_3
$(\beta La)+(\alpha Fe)+La_3Ni$

524 | $L+(\alpha Fe)\leftrightarrow La_7Ni_3+LaNi$ | U_7
$(\alpha Fe)+La_7Ni_3+LaNi$

La-Ni

1271 | e_2
$L\leftrightarrow LaNi_5+(Ni)$

1007 | p_2
$L+LaNi_5\leftrightarrow La_5Ni_{19}$

968 | p_3
$L+La_5Ni_{19}\leftrightarrow La_2Ni_7$

867 | p_5
$L+(\gamma La)\leftrightarrow(\beta La)$

796 | p_6
$L+La_2Ni_7\leftrightarrow LaNi_3$

698 | p_7
$L+LaNi_3\leftrightarrow La_7Ni_{16}$

674 | p_8
$L+La_7Ni_{16}\leftrightarrow La_2Ni_3$

658 | e_4
$L\leftrightarrow La_2Ni_3+LaNi$

534 | e_6
$L\leftrightarrow La_7Ni_3+La_3Ni$

531 | e_9
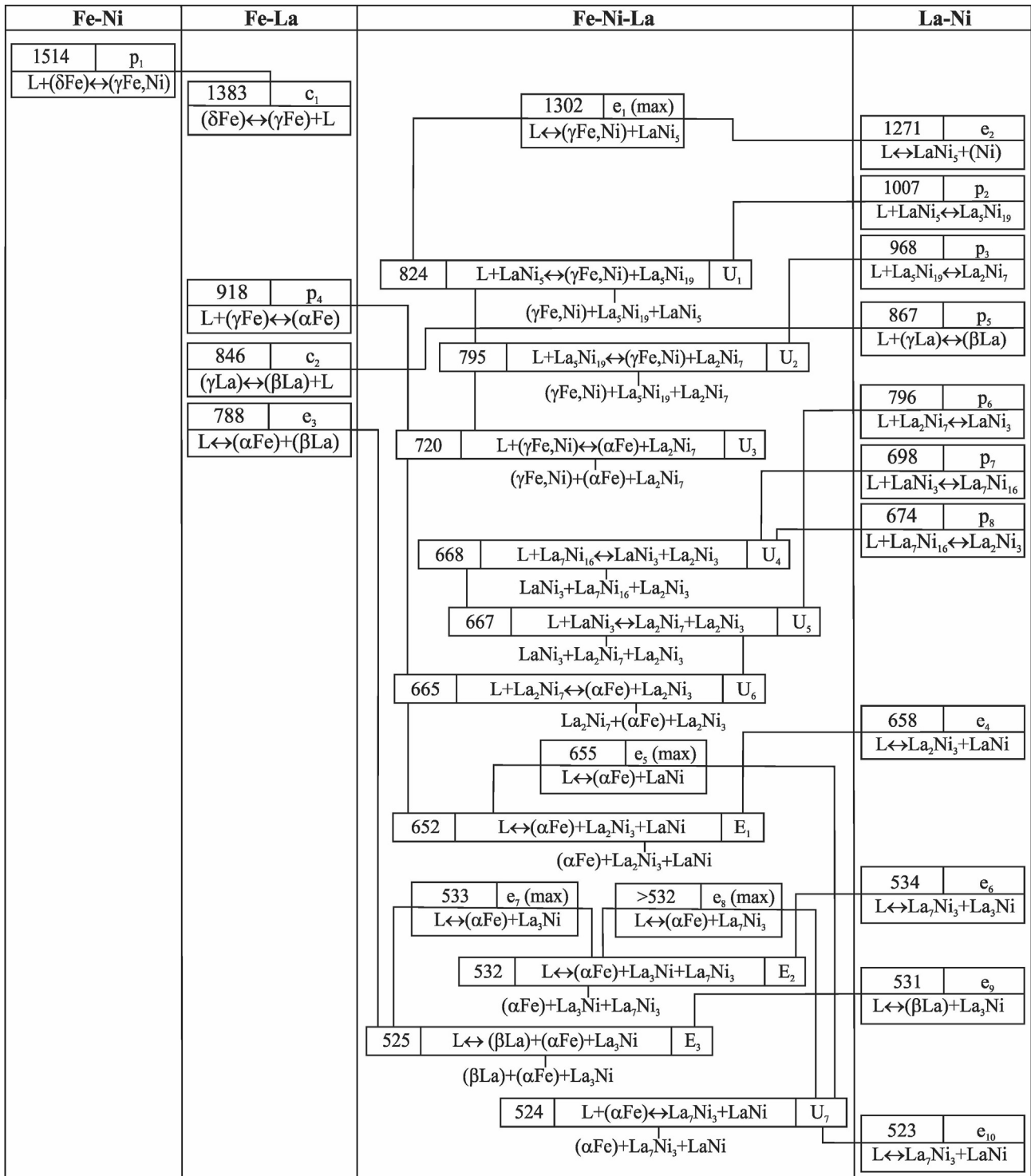$L\leftrightarrow(\beta La)+La_3Ni$

523 | e_{10}
$L\leftrightarrow La_7Ni_3+LaNi$

Fig. 10. Scheil reaction scheme for solidification of the La–Ni–Fe alloys.

$\rightleftarrows (\alpha Fe) + La_2Ni_7$, $L_{U4} + La_7Ni_{16} \rightleftarrows La_2Ni_3 + LaNi_3$, $L_{U5} + LaNi_3 \rightleftarrows La_2Ni_7 + La_2Ni_3$, $L_{U6} + La_2Ni_7 \rightleftarrows (\alpha Fe) + La_2Ni_3$, $L_{U7} + (\alpha Fe) \rightleftarrows LaNi + La_7Ni_3$, $L_{E1} \rightleftarrows (\alpha Fe) + LaNi + La_2Ni_3$, $L_{E2} \rightleftarrows (\alpha Fe) + La_3Ni + La_7Ni_3$, $L_{E3} \rightleftarrows (\alpha Fe) + La_3Ni + (\beta La)$, taking place at 824, 795, 720, 668, 667, 665, 524, 652, 532 and 525 °C, respectively.

The monovariant curves $L \rightleftarrows (Ni) + LaNi_5$, $L \rightleftarrows (\alpha Fe) + LaNi$, $L \rightleftarrows (\alpha Fe) + La_7Ni_3$ and $L \rightleftarrows (\alpha Fe) + La_3Ni$ have saddle points corresponding to the folds of maximum temperatures on the solidus

surface $(\gamma Fe,Ni) + LaNi_5$, $(\alpha Fe) + LaNi$, $(\alpha Fe) + La_3Ni$ and $(\alpha Fe) + La_7Ni_3$ at 1302, 655, 533 and > 532 °C, respectively. All invariant equilibria are summarized in Table 6. Fig. 10 shows the Scheil reaction scheme for the solidification of the La–Ni–Fe alloys.

In general, the solidus projection of the La–Ni–Fe system constructed in this work is somewhat contradictory to the isothermal sections at 400 °C [35] and 550 °C [37]. Differences can be formulated as follows:

1. The isothermal sections at $400\,^{\circ}C$ [35] and $550\,^{\circ}C$ [37] do not include the binary compound La_5Ni_{19} and consequently do not show equilibria with its participation.
2. Instead of $(\alpha Fe) + La_7Ni_{16}$ two phase equilibrium, shown by Ref. [37] at $550\,^{\circ}C$, alternative equilibrium $La_2Ni_7 + La_2Ni_3$ exists at the solidus temperature, as shown by us, and at $400\,^{\circ}C$ [35]. Possibly, between the solidus temperature and $550\,^{\circ}C$ phase transformation occurs, resulting in equilibria, established by Ref. [37]. However, this does not explain the existence equilibrium $La_2Ni_7 + La_2Ni_3$, which was found by Refs. [35] at $400\,^{\circ}C$.
3. The $LaNi_2$ compound reported in the work [35] at $400\,^{\circ}C$ cannot exist. The La_7Ni_{16} compound should exist instead of $LaNi_2$.
4. The isothermal section at $400\,^{\circ}C$ reported in the work [35] does not include the binary compound La_3Ni and consequently do not show equilibria with its participation.

5. Conclusions

The phase diagram of the binary La−Ni system is revised. Phase equilibria in the La−Ni−Fe system over the whole concentration range during solidification have been studied for the first time using DTA, X-ray diffraction, SEM and electron probe microanalysis. Liquidus and solidus projections, as well as the melting diagram and a Scheil reaction scheme were constructed for this system.

This study shows several important points:

1. The existence of nine compounds $LaNi_5$, La_5Ni_{19}, La_2Ni_7, $LaNi_3$, La_7Ni_{16}, La_2Ni_3, $LaNi$, La_7Ni_3 and La_3Ni and five eutectic reactions in the La−Ni system were confirmed. Only $LaNi_5$ phase has some homogeneity range.
2. The phases $LaNi_5$, La_5Ni_{19} and La_2Ni_7, originating from the binary La−Ni system, have the widest homogeneity ranges in the La−Ni−Fe system. At the solidus temperature these phases dissolve up to 21.9, 16.1 and 14.0 at.% Fe, respectively.
3. The liquidus surface of the La−Ni−Fe system is characterized by 13 primary solidification fields of the component-based solid solutions and solid solutions based on binary phases. The $(\gamma Fe,Ni)$-phase has the widest region of primary crystallization.
4. The solidus surface of the La−Ni−Fe system is characterized the presence of 10 three phase regions formed by invariant four-phase equilibria: three of them are of the eutectic type and the remaining are of the U-type.

CRediT authorship contribution statement

I. Fartushna: Investigation, Writing - review & editing. **M. Mardani:** Investigation, Writing - review & editing. **I. Bajenova:** Investigation, Writing - review & editing. **A. Khvan:** Conceptualization, Supervision, Writing - review & editing, Supervision, Writing - review & editing. **V. Cheverikin:** Investigation, Writing - review & editing. **K.W. Richter:** Investigation, Writing - review & editing.

Declaration of competing interest

The authors declare that they have no known competing financial interests or personal relationships that could have appeared to influence the work reported in this paper.

Acknowledgements

References

[1] K.H.J. Buschow, Intermetallic compounds of rare-earth and 3d transition metals//Reports, Prog. Phys. 40 (10) (1977) 1179−1256.
[2] F. Pourarian, A. Pedziwiatr, W.E. Wallace, Magnetic properties of RNi4Fe alloys (R = La, Ce, or Y), J. Appl. Phys. 55 (6) (1984) 1981−1983.
[3] M. Mardani, I. Fartushna, A. Khvan, V. Cheverikin, A. Dinsdale, Experimental investigation of phase transformations in the La-Fe and La-Fe-C systems, Calphad 65 (2019) 370−384.
[4] A.V. Khvan, I.V. Fartushna, M. Mardani, A.T. Dinsdale, V.V. Cheverikin, An experimental investigation of the liquidus projection in the Fe-Ce-C system, J. Alloys Compd. 651 (2015) 350−356.
[5] M. Mardani, I. Fartushna, A. Khvan, V. Cheverikin, D. Ivanov, A. Dinsdale, Phase equilibria in the Fe-Ce-C system at 1100°C, J. Alloys Compd. 730 (2018) 352−359.
[6] A.V. Khvan, M. Mardani, I.V. Fartushna, E.A. Syutkin, V.V. Cheverikin, A.T. Dinsdale, An experimental investigation of thermodynamic properties of β-Fe17Ce2, Fe2Ce, and ternary Fe13.1-11.0Mn3.9-6.0Ce2 (τ1) phase, Thermochim. Acta 672 (2019) 1−8.
[7] I. Fartushna, A. Khvan, A. Dinsdale, V. Cheverikin, Ivanov D., Kondratiev A, an experimental investigation of liquidus and solidus projections for the Fe−Mn−Ce system, J. Alloys Compd. 654 (2016) 424−434.
[8] I. Fartushna, A. Khvan, A. Dinsdale, V. Cheverikin, D. Ivanov, A. Kondratiev, Phase equilibria in the Fe−Mn−Ce system at 900°C, J. Alloys Compd. 658 (2016) 331−336.
[9] I. Fartushna, M. Mardani, A. Khvan, E. Donkor, V. Cheverikin, A. Kondratiev, A. Dinsdale, Investigation of phase equilibria in the Ce-Co-Fe system during solidification, J. Alloys Compd. 735 (2018) 1682−1693.
[10] I. Fartushna, M. Mardani, A. Khvan, V. Cheverikin, D. Ivanov, A. Kondratiev, A. Dinsdale, Phase equilibria in the Ce-Co-Fe system at 900°C, J. Alloys Compd. 765 (2018) 644−649.
[11] M. Mardani, I. Fartushna, A. Khvan, V. Cheverikin, A. Dinsdale, Experimental investigation of phase equilibria in the Ce-Fe-Ni system, J. Alloys Compd. 781 (2019) 524−540.
[12] I. Fartushna, M. Mardani, A. Khvan, V. Cheverikin, M. Gorshenkov, A. Dinsdale, Experimental investigation of phase equilibria in the Ce-Fe-Ni system at 950 and 750°C, Calphad 64 (2019) 284−291.
[13] I. Fartushna, M. Mardani, A. Khvan, V. Cheverikin, A. Kondratiev, Experimental investigation of Fe-Co-La system: liquidus and solidus projections, J. Phase Equilibria Diffus. (2020), https://doi.org/10.1007/s11669-020-00800-w.
[14] I. Fartushna, M. Mardani, A. Khvan, V. Cheverikin, A. Kondratiev, Experimental investigation of phase equilibria in the Co-Fe-La system at 600 and 500°C, Calphad (2020) (accepted).
[15] G. Cacciamani, A. Dinsdale, M. Palumbo, A. Pasturel, The Fe−Ni system: thermodynamic modelling assisted by atomistic calculations, Intermetallics 18 (6) (2010) 1148−1162.
[16] P. Rossiter, R. Jago, Towards a true Fe-Ni phase diagram, Mater. Res. Soc. Symp. Proc. 21 (1984) 407−411.
[17] C. Yang, D. Williams, J. Goldstein, A revision of the Fe-Ni phase diagram at low temperatures (<400°C), J. Phase Equil. 17 (1996) 522−531.
[18] R. Vogel, W. Fülling, Über die Systeme Cer-Nickel, Lanthan-Nickel, Praseodym-Nickel und Cer-Kobalt, Metallforschung 2 (1947) 97−103 (in German).
[19] K.H. Buschow, H.H. Van Mal, Phase relations and hydrogen absorption in the lanthanum-nickel system, J. Less Common Met. 29 (2) (1972) 203−210.
[20] V. Ivanchenko, G. Kobzenko, V. Svechnikov, Phase equilibria in the La-Ni system, Dopov. Akad. Nauk. Ukr. RSR 1 (1982) 83−86 (in Russian).
[21] D. Zhang, J. Tang, K.A. Gschneidner, A redetermination of the La-Ni phase diagram from LaNi to LaNi5 (50 to 83.3 at.% Ni), J. Less Common. Met. 169 (1991) 45−53.
[22] J. Dischinger, H.J. Schaller, On the constitution and thermodynamics of Ni−La alloys, J. Alloys Compd. 312 (2000) 201−210.
[23] Z. Du, D. Wang, W. Zhang, Thermodynamic assessment of the La-Ni system, J. Alloys Compd. 264 (1−2) (1998) 209−213.
[24] L. Liu, Z. Jin, Thermodynamic reassessment of the La-Ni system, Z. Metallkd 91 (9) (2000) 739−743.
[25] X.H. An, Q.F. Gu, J.Y. Zhang, S.L. Chen, X.B. Yu, Q. Li, Experimental investigation and thermodynamic reassessment of La-Ni and LaNi5−H systems, Calphad 40 (2013) 48−55.
[26] K.A. Gschneidner Jr., Rare Earth Alloy, D. Van Nostrand, NY, 1961.
[27] A.V. Virkar, A. Raman, Crystal structures of AB3 and A2B7 rare earth-nickel phases, J. Less Common. Met. 18 (1969) 59−66.
[28] J.H.N. Van Vucht, K.H.J. Buschow, The crystal structure of La2Ni3, J. Less Common Met. 46 (1) (1976) 133−138.
[29] A.V. Klimyenko, J. Seuntjens, L.L. Miller, B.J. Beaudry, R.A. Jacobson, K.A. Gschneidner Jr., Structure of LaNi2.286 and the La-Ni system from LaNi1.75 to LaNi2.50, J. Less Common Met. 144 (1) (1988) 133−141.
[30] T. Yamamoto, H. Inui, M. Yamaguchi, K. Sato, S. Fujitani, I. Yonezu, K. Nishio, Microstructures and hydrogen absorption/desorption properties of LaNi alloys in the composition range of La-77.8−83.2 at.% Ni, Acta Mater. 45 (12) (1997) 5213−5221.
[31] H. Inui, T. Yamamoto, D. Zhang, M. Yamaguchi, Microstructures and defect structures in intermetallic compounds in the La−Ni alloy system, J. Alloys Compd. 293−295 (1999) 140−145.

[32] A. Férey, F. Cuevas, M. Latroche, B. Knosp, P. Bernard, Elaboration and characterization of magnesium-substituted La_5Ni_{19} hydride forming alloys as active materials for negative electrode in Ni-MH battery, Electrochim. Acta 54 (6) (2009) 1710−1714.

[33] Z. Di, T. Yamamoto, H. Inui, M. Yamaguchi, Characterization of stacking faults on basal planes in intermetallic compounds La_5Ni_{19} and La_2Ni_7, Intermetallics 8 (2000) 391−397.

[34] G. Qi, Z. Li, K. Itagaki, A. Yazawa, High temperature phase relations in Ni−RE (RE= La, Ce, Pr, Nd) binary and ternary alloy systems, Mater. Trans., JIM 30 (8) (1989) 583−593.

[35] O. Charczenko, O.I. Bodak, E. Hladyszewskyi, L. Bondarenko, Phase Equilibria in La-Fe-Ni System, Ann. Univers. M. Curie-Sklodowska, Lublin-Polonia, Sect. AA 31-32, 1976/1977, pp. 131−136 (in Polish).

[36] C. Wang, S. Dai, Phase equilibrium and hydrogen absorption of Ni-Fe-16.7 at.% La system, Acta Metall. Sin. 22 (6) (1986) 264−367 (in Chinese).

[37] H. Zhou, Y. Zhu, J. Liu, Y. Zhuang, S. Yuan, Isothermal sections (400 and 550° C) of the phase diagram of the La-Ni-Fe ternary system, J. Alloys Compd. 345 (1−2) (2002) 167−169.

[38] W. Kraus, G. Nolze, POWDERCELL, Rev. 1.8a, Federal Institute for Materials Research and Testing (BAM), Berlin, 1996.

[39] WINXPOW Software, Stoe & Cie GmbH Darmstadt, 1998.

[40] T.B. Massalski (Ed.), Binary Alloy Phase Diagrams, second ed., ASM International, Metals Park, OH, 1990.

[41] V. Paul-Boncour, A. Lindbaum, Ab initio calculations on the formation of La1-xNi2 compounds, J. Phys. Condens. Matter 14 (15) (2002) 3921.

[42] A.E. Dwight, R.A. Conner Jr., J.W. Downey, Equiatomic compounds of the transition and lanthanide elements with Rh, Ir, Ni and Pt, Acta Crystallogr. 18 (1965) 835−839.

[43] G.L. Olcese, Crystal structure and magnetic properties of some 7:3 binary phases between lanthanides and metals of the 8th group, J. Less Common. Met. 33 (1973) 71−81.

[44] P. Fischer, W. Hälg, L. Schlapbach, K. Yvon, Neutron and X-ray diffraction investigation of deuterium storage in La_7Ni_3, J. Less Common Met. 60 (1) (1978) 1−9.

[45] R. Lemaire, D. Paccard, Structure cristallographique des composés intermétalliques T_3Ni, T désignant un métal de terre rare ou l'yttrium, Bull. Mineral. 90 (3) (1967) 311−315.

[46] C.S. Garde, J. Ray, Magnetic and superconducting behaviour of the R_3Ni (R= La, Pr, Gd, Tb, Ho and Er) systems, J. Phys. Condens. Matter 9 (1997) 7419−7434.